AMERICAN SOCIETY FOR MICROBIOLOGY | Journal of Virology®

STRUCTURE AND ASSEMBLY

Qualitative Differences in Capsidless L-Particles Released as a By-Product of Bovine Herpesvirus 1 and Herpes Simplex Virus 1 Infections

Tiffany Russell,[a] Ben Bleasdale,[b] Michael Hollinshead,[b]* Gillian Elliott[a]

[a]Department of Microbial Sciences, Faculty of Health and Medical Sciences, University of Surrey, Guildford, United Kingdom

[b]Section of Virology, Imperial College London, London, United Kingdom

ABSTRACT Despite differences in the pathogenesis and host range of alphaherpesviruses, many stages of their morphogenesis are thought to be conserved. Here, an ultrastructural study of bovine herpesvirus 1 (BoHV-1) envelopment revealed profiles similar to those previously found for herpes simplex virus 1 (HSV-1), with BoHV-1 capsids associating with endocytic tubules. Consistent with the similarity of their genomes and envelopment strategies, the proteomic compositions of BoHV-1 and HSV-1 virions were also comparable. However, BoHV-1 morphogenesis exhibited a diversity in envelopment events. First, heterogeneous primary envelopment profiles were readily detectable at the inner nuclear membrane of BoHV-1-infected cells. Second, the BoHV-1 progeny comprised not just full virions but also an abundance of capsidless, noninfectious light particles (L-particles) that were released from the infected cells in numbers similar to those of virions and in the absence of DNA replication. Proteomic analysis of BoHV-1 L-particles and the much less abundant HSV-1 L-particles revealed that they contained the same complement of envelope proteins as virions but showed variations in tegument content. In the case of HSV-1, the U_L46 tegument protein was reproducibly found to be >6-fold enriched in HSV-1 L-particles. More strikingly, the tegument proteins U_L36, U_L37, U_L21, and U_L16 were depleted in BoHV-1 but not HSV-1 L-particles. We propose that these combined differences reflect the presence of truly segregated "inner" and "outer" teguments in BoHV-1, making it a critical system for studying the structure and process of tegumentation and envelopment.

IMPORTANCE The alphaherpesvirus family includes viruses that infect humans and animals. Hence, not only do they have a significant impact on human health, but they also have a substantial economic impact on the farming industry. While the pathogenic manifestations of the individual viruses differ from host to host, their relative genetic compositions suggest similarity at the molecular level. This study provides a side-by-side comparison of the particle outputs from the major human pathogen HSV-1 and the veterinary pathogen BoHV-1. Ultrastructural and proteomic analyses have revealed that both viruses have broadly similar morphogenesis profiles and infectious virus compositions. However, the demonstration that BoHV-1 has the capacity to generate vast numbers of capsidless enveloped particles that differ from those produced by HSV-1 in composition implies a divergence in the cell biology of these viruses that impacts our general understanding of alphaherpesvirus morphogenesis.

KEYWORDS BoHV-1, envelopment, HSV-1, L-particles, morphogenesis, tegument

The alphaherpesvirus subfamily comprises a group of complex viruses that includes important human and animal pathogens, such as herpes simplex virus 1 (HSV-1) and bovine herpesvirus 1 (BoHV-1). Such viruses have a significant impact on human or animal health (1, 2) and in the case of agricultural infections can have a substantial

Received 23 July 2018 **Accepted** 23 August 2018

Accepted manuscript posted online 5 September 2018

Citation Russell T, Bleasdale B, Hollinshead M, Elliott G. 2018. Qualitative differences in capsidless L-particles released as a by-product of bovine herpesvirus 1 and herpes simplex virus 1 infections. J Virol 92:e01259-18. https://doi.org/10.1128/JVI.01259-18.

Editor Richard M. Longnecker, Northwestern University

Address correspondence to Gillian Elliott, g.elliott@surrey.ac.uk.

* Present address: Michael Hollinshead, Department of Pathology, University of Cambridge, Cambridge, United Kingdom.

T.R. and B.B. contributed equally to the work.

economic impact (3, 4). Despite these viruses showing a diverse range of clinical manifestations (5, 6), they show conservation in genome composition and virion morphology (7, 8). The alphaherpesvirus particle consists of the DNA-containing capsid surrounded by a proteinaceous layer known as the tegument, comprised of over 20 virus-encoded proteins and multiple cell proteins, which links the capsid with its host membrane-derived envelope containing multiple virus-encoded glycoproteins (9, 10). While studies on virion assembly have tended to center around HSV-1 and pseudorabies virus (PRV), there is growing interest in utilizing other alphaherpesviruses to enhance our understanding of specific morphogenesis details that are still missing.

The currently favored model for assembly of the complex virion is termed the envelopment-deenvelopment-reenvelopment model, in which capsids form in the nucleus and bud through the inner nuclear membrane (INM) as a primary virion (11–13). The virus-encoded machinery required for this envelopment, termed the nuclear egress complex or NEC, consists of U_L31 and U_L34, considered to be the tegument and envelope of the primary virion (14). This machinery is autonomous and can function when expressed in isolation or even *in vitro* (15, 16). The primary envelope is lost by fusion with the outer nuclear membrane (ONM), releasing naked capsids into the cytosol (11, 12). This cytoplasmic capsid is subsequently enveloped in cellular membranes together with the complement of tegument proteins to form the mature virion.

The cellular location of alphaherpesvirus secondary envelopment has been a point of contention for many years. For HSV-1 at least, in a model derived from ultrastructural and Rab GTPase depletion studies, we have proposed that clathrin-mediated endocytosis of tubules from the plasma membrane provides the main source of the HSV-1 envelope, with a concomitant cycling of virus envelope proteins through the plasma membrane to the endocytic wrapping tubules (17). Virus egress would then result from the natural recycling of these membranes to the cell surface. This model is in agreement with previous studies from others (18) and has been supported by more recent studies showing that glycoproteins must be transported to the plasma membrane prior to envelopment taking place (19, 20).

One idiosyncratic feature of the alphaherpesvirus envelopment pathway that has not been fully explored for understanding the molecular mechanisms involved in envelopment is the production of noninfectious light particles (L-particles) that lack the viral DNA-containing capsid but contain an enveloped tegument structure (21–26). These L-particles could also help in understanding the process of tegumentation, i.e., where and when the numerous tegument proteins are recruited to the assembling virion. Combinations of genetic and protein-protein interaction studies have led to the concept of inner and outer tegument proteins, with inner tegument proteins (such as U_L36 and U_L37) linking the capsid to the tegument and outer tegument proteins (such as U_L49) linking the tegument to the envelope (27). Inner tegument proteins would hence be assembled onto the capsid at any point prior to envelopment, with some evidence suggesting that U_L36 may already be present on intranuclear capsids (28, 29). While outer tegument proteins are proposed to be recruited to the envelope by interactions with the cytoplasmic tails of glycoproteins, conclusive evidence for such recruitment is still limited, with only two examples, U_L11 and U_L49, so far definitively shown to be assembled in this way (30–33). This issue is further compounded by the fact that many of the tegument proteins, even the major ones such as U_L47 and U_L49, which are considered to be structurally important, are dispensable for virus growth and therefore not required for virion formation (34–37). The assembly of tegument proteins into L-particles may offer a different route to understanding the molecular interactions that occur during alphaherpesvirus envelopment.

In this study, we employed a dual approach based on ultrastructural studies of morphogenesis and virion proteomics to carry out comparative studies of HSV-1 and BoHV-1 morphogenesis. We demonstrate that BoHV-1 assembly utilizes recently endocytosed material for envelopment in a manner analogous to that of HSV-1, while side-by-side proteomic analysis also confirmed similar compositions for HSV-1 and

BoHV-1 virions. BoHV-1 was seen to produce large numbers of capsidless L-particles that were released in equivalent numbers to infectious virions. We report the first proteomic analysis of alphaherpesvirus L-particles indicating that the BoHV-1 but not the HSV-1 L-particles were depleted for proteins that are commonly classified as part of the inner tegument. These results reveal differences in the particle outputs from these two viruses that make BoHV-1 L-particles a useful model with which to study tegumentation and envelopment.

RESULTS

BoHV-1 capsids are wrapped in endocytic membranes. We have previously shown that HSV-1 virions acquire their final envelopes from glycoprotein-containing endocytic tubular membranes that have been recently retrieved from the cytoplasmic membrane, by using horseradish peroxide (HRP) to label fluid-phase endocytic events in infected cells (17). To investigate BoHV-1 envelopment, we therefore carried out the same labeling of bovine MDBK cells, one of the few cell types in which BoHV-1 replicates, 12 h after infection at a multiplicity of 2. These studies revealed the presence of many HRP-labeled endocytic tubules with a curved profile in the cytoplasm (Fig. 1A to C). These endocytic tubules frequently carried a budded terminal domain (Fig. 1B, arrowheads), which had an indistinct peripheral coating when observed at higher magnification (Fig. 1C, arrowheads), consistent with the appearance of clathrin coats, as we have observed previously (17). Virus capsids were frequently found in tight association with these endocytic tubules in the cytoplasm of the infected cells (Fig. 1D to H). Furthermore, many tubules that were associated with capsids retained the budded terminal domain, consistent with a clathrin coat (Fig. 1G and H, arrowheads). Fully enveloped virions wrapped in double membranes were detected in the cytoplasm (Fig. 1I), while particles enclosed in a single membrane were observed outside the cell, consistent with our previous HSV-1 studies (Fig. 1J).

Comparative proteomic analysis of extracellular BoHV-1 and HSV-1 virions. We next determined the relative protein contents of HSV-1 and BoHV-1 virions by isolating extracellular virions from infected cultures of physiologically relevant cells, namely, the HaCaT human keratinocyte cell line and the bovine epithelial MDBK cell line, respectively. The virions were banded on a Ficoll gradient, and approximately equivalent numbers of virions were solubilized and separated by SDS-PAGE, followed by staining with Coomassie blue to confirm the presence and purity of virions (Fig. 2A). Based on their characteristic sizes and previous studies, several key components of virions were identified, including the major capsid protein (VP5) and the tegument proteins U_L36, U_L47, U_L48, and U_L49. Of note, all these proteins, with the exception of U_L47, were present at equivalent levels in both types of virions (Fig. 2A). In the case of U_L47, in BoHV-1, this protein (also known as VP8) is known to be packaged in unusually large amounts (38). The BoHV-1 and HSV-1 virion proteins were subsequently separated by SDS-PAGE and subjected to in-gel tryptic digestion, followed by fractionation using a nanoscale high-performance liquid chromatography (nano-HPLC) system and tandem mass spectrometry (MS/MS) to identify both virus and host cell proteins.

Using a conservative false discovery rate (FDR) of less than 1%, 51 virus and 488 host cell proteins were identified in HSV-1 virions, and 51 virus and 883 host cell proteins were identified in BoHV-1 (Fig. 2B). When considering those proteins predicted to be conserved based on genome homology, the viral protein compositions of BoHV-1 and HSV-1 virions were broadly similar, with 42 virus proteins identified in virions of both viruses (Fig. 2C). Of the nine virus proteins that were uniquely identified in BoHV-1 virions, CIRC, $U_S1.67$, and $U_L3.5$ can be accounted for by a lack of conservation of these open reading frames within the HSV-1 genome. Likewise, five of the nine proteins uniquely identified in HSV-1 virions are not conserved in the BoHV-1 genome (U_L45, U_L55, U_L56, U_S10, and U_S11). The full lists of virus proteins that were identified in HSV-1 and BoHV-1 virions are presented in Tables 1 and 2, respectively, organized according to their proposed localization within the virion (8, 10), with a side-by-side comparison provided in Table 3.

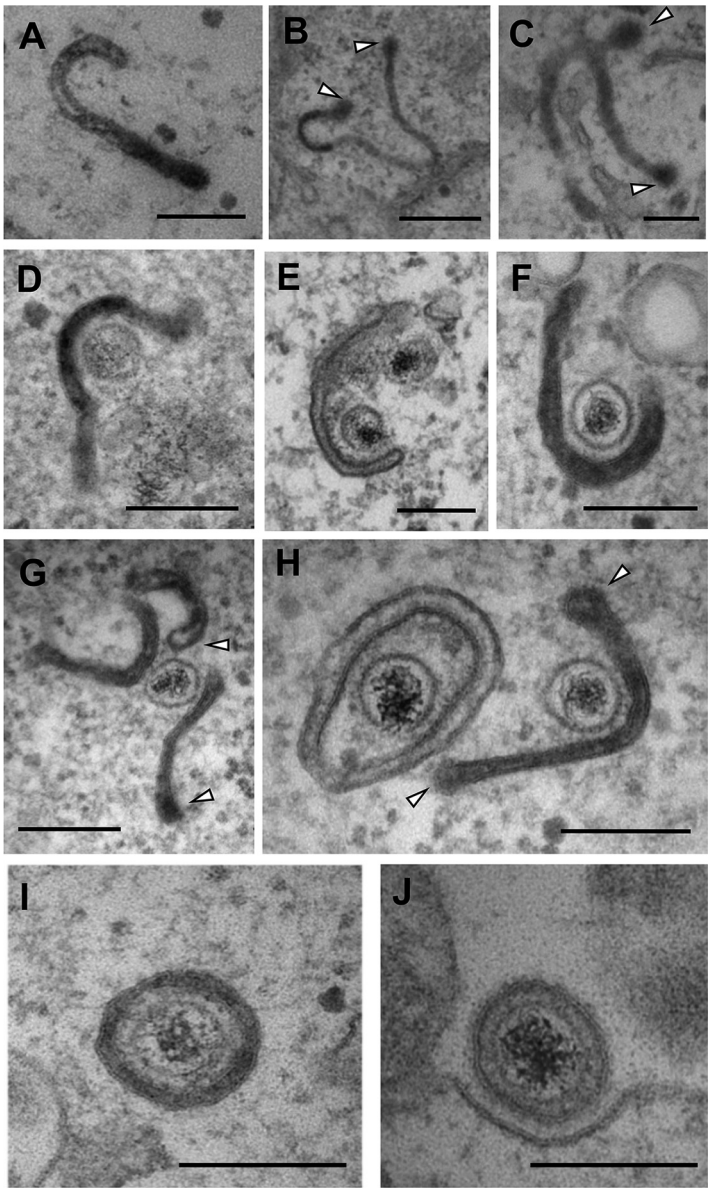

FIG 1 BoHV-1 capsids are wrapped in tubular endocytic membranes. MDBK cells were infected at a multiplicity of infection (MOI) of 5 with BoHV-1, and HRP was added to the medium for 30 min at 12 h postinfection (hpi). Samples were fixed, processed, and imaged by transmission electron microscopy. White arrows in panels B, C, G, and H indicate the budded terminal domains of endocytic tubules. Bars = 500 nm (B) and 200 nm (A and C to J).

The viral content of HSV-1 extracellular virions was very similar to that previously reported by Loret and colleagues (10), confirming the presence of four novel virion components (U_L7, U_L23, U_L50, and U_L55) identified in that study, although we failed to detect ICP34.5, which has also been characterized elsewhere as a virion component (39). Likewise, the virus protein content of BoHV-1 virions was similar to that previously reported by Barber and colleagues (8). We also identified 20 proteins in BoHV-1 virions (Table 2) and 10 proteins in HSV-1 virions (Table 1) that were not identified in those original studies (8, 10). The low protein score and poor peptide coverage of these proteins suggest that they could be nonspecific, low-level contamination from cells that had been picked up due to the increased sensitivity of mass spectrometry. However, detection in virions from both the viruses and/or previous characterization of these proteins as virion constituents suggests that at least some of them, such as U_S11 in HSV-1, are likely to be low-abundance constituents of the virion (40).

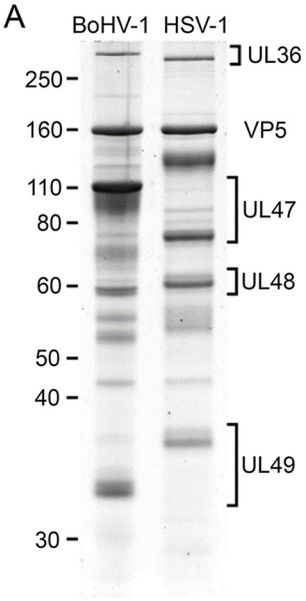

B

		HSV-1	BoHV-1
Number of proteins encoded in genome		73	68
Number of viral proteins identified in virions	<1% FDR	51	51
	<5% FDR	57	55
Number of viral proteins not identified in virions	<5% FDR	16	13
Number of cell proteins identified in virions	<1% FDR	488	883
	<5% FDR	1176	1888

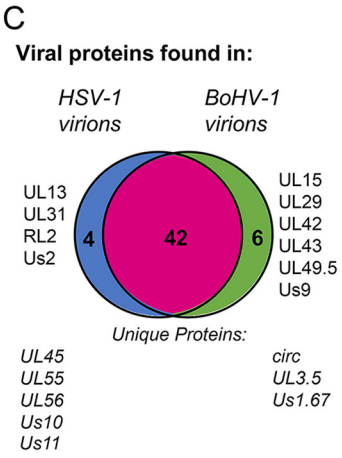

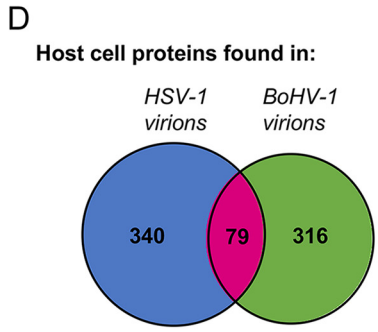

FIG 2 Purification and proteomic characterization of extracellular HSV-1 and BoHV-1 virions. Confluent monolayers of HaCaT cells and MDBK cells were infected with HSV-1 and BoHV-1, respectively; at full cytopathic effect, cells were harvested; and virions were isolated by separation on a 5 to 15% Ficoll gradient. (A) BoHV-1 and HSV-1 virions were separated by 10% SDS-PAGE and stained with Coomassie blue. Size markers are shown in kilodaltons. (B) Summary of the numbers of proteins identified in HSV-1 and BoHV-1 virions, at <5% and <1% FDRs. (C and D) Venn diagrams showing the overlap in virus proteins (C) and host cell proteins (D) identified in HSV-1 and BoHV-1 virions.

When considering those human host cell proteins for which there is a known bovine homologue, only a quarter of the host cell proteins identified was shared between the two viruses, variability which could be a consequence of isolating the virions from different cell types (Fig. 2D). A selection of the proteins that were identified in both BoHV-1 and HSV-1 virions is shown in Table 4, with the full list of host cell proteins identified in BoHV-1 and HSV-1 virions presented Tables S1 and S2 and a comparison presented in Table S3 in the supplemental material. While many of these proteins have been previously identified within herpesvirus virions (8, 10, 41), the specificity of their packaging remains to be determined. One potential explanation for the presence of so many cell proteins in our preparations is that exosomes have been purified along with our virions. While some exosomal markers (42) are present within our top cell protein hits (annexin A2, cofilin, heat shock protein 70, and GAPDH [glyceraldehyde-3-phosphate dehydrogenase]), it would be difficult to say with confidence that exosomes are present. Moreover, because many of these proteins are known to be among the most abundant proteins within the cell according to previously reported protein abundance data (43), another interpretation of their presence is that their recruitment is simply a reflection of local concentration at the site of envelopment rather than specific incorporation into the virion. In light of this uncertainty, we have not explored the packaging of cellular proteins further in this study.

A range of envelopment events in BoHV-1-infected cells. When examining BoHV-1-infected MDBK cells by standard transmission electron microscopy (TEM), we noted that these cells contained many more detectable primary envelopment events at the inner nuclear membrane (INM) than we had found in our previous studies of HSV-1-infected primary human fibroblasts (17). Assembled capsids surrounded by a distinct electron-dense primary envelope located in the perinuclear space between the

TABLE 1 Virus proteins detected in extracellularHSV-1 virions[a]

Location	Accession	Protein Name in HSV-1	Gene Name in HSV-1	Protein score	Coverage	# Unique Peptides	Previously identified in virions
Glycoproteins	P10185	gL	U_L1	146.61	36.61	7	Y
	P04288	gM	U_L10	258.23	18.82	6	Y
	P06477	gH	U_L22	633.87	48.09	38	Y
	P10211	gB	U_L27	1545.66	60.18	60	Y
	P10228	gC	U_L44	888.89	29.16	16	Y
	P68331	gK	U_L53	43.10	21.89	6	N
	P06484	gG	U_S4	37.38	11.76	3	Y
	Q69091	gD	U_S6	838.27	54.31	24	Y
	P06487	gI	U_S7	230.02	35.13	9	Y
	P04488	gE	U_S8	608.29	59.09	28	Y
Other envelope proteins	P10204	U_L20	U_L20	7.53	7.66	2	N
	P10218	U_L34	U_L34	10.50	12.36	3	N
	P10229	U_L45	U_L45	208.58	38.95	5	Y
Capsid proteins	P10190	U_L6	U_L6	98.86	36.98	21	Y
	P10201	U_L17	U_L17	320.27	48.65	25	Y
	P10202	VP23	U_L18	681.81	69.81	15	Y
	P06491	VP5 or ICP5	U_L19	4451.50	66.01	90	Y
	P10209	U_L25	U_L25	680.96	72.59	34	Y
	P10210	VP24	U_L26	402.09	34.49	19	Y
	P10219	VP26	U_L35	181.81	75.89	5	Y
	P32888	VP19c	U_L38	806.37	53.76	28	Y
Tegument proteins	P08393	ICP0	R_L2	118.41	34.45	18	Y
	P10191	U_L7	U_L7	138.44	44.93	10	Y
	P04289	U_L11	U_L11	26.60	20.83	2	Y
	P04290	U_L13	U_L13	57.69	34.75	10	Y
	P04291	U_L14	U_L14	29.97	26.03	8	Y
	P10200	U_L16	U_L16	477.73	72.65	18	Y
	P10205	U_L21	U_L21	561.35	74.39	33	Y
	P03176	TK	U_L23	56.61	19.95	6	Y
	P10215	U_L31	U_L31	9.79	9.80	2	N
	P10220	U_L36	U_L36	1969.93	49.08	120	Y
	P10221	U_L37	U_L37	1206.35	71.06	62	Y
	P10225	VHS	U_L41	384.53	58.49	23	Y
	P10230	VP11/12	U_L46	395.80	57.94	31	Y
	P10231	VP13/14	U_L47	1912.27	86.44	62	Y
	P06492	VP16 or ICP25	U_L48	1029.46	49.18	26	Y
	P10233	VP22	U_L49	1342.28	72.76	21	Y
	P10234	U_L50	U_L50	147.57	51.75	13	Y
	P10235	U_L51	U_L51	141.66	52.87	8	Y
	P10239	U_L55	U_L55	54.96	69.35	8	Y
	P10240	U_L56	U_L56	35.82	35.53	5	N
	P08392	ICP4	R_S1	129.86	36.29	31	Y
	P04485	ICP22	U_S1	4.62	4.29	2	Y
	P06485	U_S2	U_S2	98.11	51.20	9	Y
	P04413	U_S3	U_S3	29.55	25.99	7	Y
	P06486	U_S10	U_S10	100.01	39.74	12	Y
	P04487	U_S11	U_S11	66.41	28.57	4	N
Other proteins	P10186	U_L2	U_L2	13.77	14.37	5	N
	P08543	ICP6	U_L39	183.47	39.05	36	N
	P10224	ICP10	U_L40	30.61	35.00	9	N
	P10238	ICP27	U_L54	4.97	7.81	3	N

[a]Shown are virus proteins identified based on a <1% FDR. Location is based on that described by Loret et al. (10), and detection in that previous study is indicated. The protein score reflects the number of peptides, abundance, and protein size to give a degree of confidence in protein identification. Coverage is calculated based on peptides identified within each protein. A side-by-side comparison of HSV-1 and BoHV-1 virions is presented in Table 3. Accession numbers were acquired from the UniProt human herpesvirus 1 (strain 17) database (https://www.uniprot.org/proteomes/UP000009294).

INM and the outer nuclear membrane (ONM) were frequently observed (Fig. 3A). These primary virions either contained packaged DNA (Fig. 3A, top) or were empty of DNA (Fig. 3A, bottom). Three budding events lacking DNA were readily identified: budding of what appear to be B capsids (Fig. 3B, white arrow) and A capsids (Fig. 3B, white arrow

TABLE 2 Virus proteins detected in extracellular BoHV-1 virions[a]

Location	Accession	Protein Name in BoHV-1	Gene Name in BoHV-1	Protein score	Coverage	# Unique Peptides	Previously identified within virions
Glycoproteins	A0A089N804	gL	U_L1	414.78	74.68	13	Y
	A0A089N7Z6	gM	U_L10	356.28	17.03	6	Y
	A0A089N2B7	gH	U_L22	1687.86	43.71	29	Y
	A0A089N646	gB	U_L27	4314.66	56.27	57	Y
	A0A089N7W5	gC	U_L44	4156.38	41.93	32	Y
	A0A089N7V8	gN	$U_L49.5$	267.97	36.46	6	N
	A0A089PGF7	gK	U_L53	261.29	42.60	15	N
	A0A089N688	gG	U_S4	1273.82	40.77	13	Y
	A0A089N2E3	gD	U_S6	1083.11	45.56	19	Y
	A0A089N3W4	gI	U_S7	514.34	35.08	10	Y
	A0A089N810	gE	U_S8	1052.01	38.09	17	Y
Other envelope proteins	A0A089N7Y8	U_L20	U_L20	38.69	29.87	6	N
	A0A089N7X5	U_L34	U_L34	12.27	17.42	3	N
	A0A089PGG6	U_L43	U_L43	28.85	12.96	3	N
Capsid proteins	A0A089N3V3	Portal protein	U_L6	16.77	8.72	5	Y
	A0A089N657	Triplex capsid protein 2	U_L18	370.95	54.75	15	Y
	A0A089PGI7	Major capsid protein	U_L19	2047.85	71.85	71	Y
	A0A089N3T6	Capsid scaffolding protein	U_L26	274.55	28.14	14	Y
	A0A089N3S8	Small capsomere interacting protein	U_L35	196.82	70.97	7	N
	A0A089PGH0	Triplex capsid protein 1	U_L38	561.83	57.89	21	Y
Tegument proteins	A0A089N3R1	Myristylated tegument protein CIRC	circ	308.90	40.24	8	Y
	A0A089N675	Protein V5V	$U_L3.5$	1335.08	69.05	11	Y
	A0A089N2C9	Cytoplasmic envelopment protein 1	U_L7	85.65	53.00	11	N
	A0A089N3U9	Cytoplasmic envelopment protein 3	U_L11	8.72	32.58	2	N
	A0A089PGJ2	U_L14	U_L14	62.41	21.88	5	N
	A0A089N7Z2	U_L16	U_L16	532.01	77.26	23	Y
	A0A089N3U4	CVC1	U_L17	329.54	52.06	25	Y
	A0A089N3U0	U_L21	U_L21	448.59	56.57	24	Y
	A0A089N652	TK	U_L23	14.89	6.69	2	N
	A0A089N7Y3	CVC2	U_L25	374.44	53.18	25	Y
	A0A089N2A4	Large tegument protein	U_L36	1047.98	36.32	85	Y
	A0A089N634	U_L37	U_L37	442.33	57.64	45	Y
	A0A089N2A0	Host shutoff protein	U_L41	457.65	50.98	22	Y
	A0A089N629	DNA polymerase processivity subunit	U_L42	107.51	50.98	15	Y
	A0A089N3R8	VP11/12	U_L46	538.88	38.28	21	Y
	A0A089N295	VP8	U_L47	3286.98	69.23	39	Y
	A0A089N623	VP16 or ICP25	U_L48	1587.92	53.06	23	Y
	A0A089PGG2	VP22	U_L49	1289.80	70.93	17	Y
	A0A089N3R5	Deoxyuridine 5'-triphosphate nucleotidohydrolase	U_L50	95.07	51.08	11	N
	A0A089N291	U_L51	U_L51	175.12	55.97	11	N
	A0A089N7V2	Multifunctional expression regulator	U_L54	17.14	12.75	3	Y
	A0A089N2E7	BICP4	R_S1	207.03	32.76	32	N
	A0A089N2D8	ICP22	U_S1	30.32	17.88	5	N
	A0A089N3W0	Virion protein	$U_S1.67$	118.54	56.79	10	Y
	A0A089PGK8	Serine/threonine protein kinase U_S3	U_S3	93.22	35.91	9	Y
	A0A089PGL4	Membrane protein U_S9	U_S9	6.29	38.89	2	N
Unknown	A0A089N3V6	Uracil DNA glycosylase	U_L2	18.48	35.29	5	N
	A0A089N2C2	Tripartite terminase subunit 3	U_L15	10.70	4.49	3	N
	A0A089N7X9	Major DNA binding protein	U_L29	13.30	5.16	5	N
	A0A089N7X0	Ribonucleoside-diphosphate reductase large subunit	U_L39	10.91	8.64	5	N
	A0A089N3S3	Ribonucleoside-diphosphate reductase small subunit	U_L40	28.85	24.44	6	N

[a]Virus proteins were identified based on a <1% FDR. Location is based on that described by Barber et al. (8) or as expected based on the localization of homologous HSV-1 proteins, and detection in that previous study is indicated. The protein score reflects the number of peptides, abundance, and protein size to give a degree of confidence in protein identification. Coverage is calculated based on peptides identified within each protein. A side-by-side comparison of HSV-1 and BoHV-1 virions is presented in Table 3. Accession numbers were acquired from the UniProt bovine herpesvirus 1 (strain K22) database (https://www.uniprot.org/proteomes/UP000170085).

with black outline) and membrane budding in the complete absence of a capsid (Fig. 3B, black arrows). Despite variations in cargo, each budding event involved similar INM curvatures, producing perinuclear vesicles of comparable diameters, and all events displayed an electron-dense coating on the inside surface of the curved

TABLE 3 Comparison of BoHV-1 and HSV-1 virion compositions[a]

Location	Protein Name in HSV-1	Gene Name in HSV-1	Found in HSV-1 and BoHV-1	HSV-1 Protein score	BoHV-1 Protein score
Glycoproteins	gL	U_L1	Yes	146.61	414.78
	gM	U_L10	Yes	258.23	356.28
	gH	U_L22	Yes	633.87	1687.86
	gB	U_L27	Yes	1545.66	4314.66
	gC	U_L44	Yes	888.89	4156.38
	gN	$U_L49.5$	Yes		267.97
	gK	U_L53	Yes	43.10	261.29
	gG	U_S4	Yes	37.38	1273.82
	gD	U_S6	Yes	838.27	1083.11
	gI	U_S7	Yes	230.02	514.34
	gE	U_S8	Yes	608.29	1052.01
Other envelope proteins	U_L20	U_L20	Yes	7.53	38.69
	U_L34	U_L34	Yes	10.50	12.27
	U_L43	U_L43	Yes		28.85
	U_L45	U_L45	No	208.58	
Capsid proteins	U_L6	U_L6	Yes	98.86	16.77
	U_L17	U_L17	Yes	320.27	329.54
	VP23	U_L18	Yes	681.81	370.95
	VP5 or ICP5	U_L19	Yes	4451.50	2047.85
	U_L25	U_L25	Yes	680.96	374.44
	VP24	U_L26	Yes	402.09	274.55
	VP26	U_L35	Yes	181.81	196.82
	VP19c	U_L38	Yes	806.37	561.83
Tegument proteins	ICP0	R_L2	Yes	118.41	
	U_L7	U_L7	Yes	138.44	85.65
	U_L11	U_L11	Yes	26.60	8.72
	U_L13	U_L13	Yes	57.69	
	U_L14	U_L14	Yes	29.97	62.41
	U_L16	U_L16	Yes	477.73	532.01
	U_L21	U_L21	Yes	561.35	448.59
	TK	U_L23	Yes	56.61	14.89
	U_L31	U_L31	Yes	9.79	
	U_L36	U_L36	Yes	1969.93	1047.98
	ICP32	U_L37	Yes	1206.35	442.33
	VHS	U_L41	Yes	384.53	457.65
	VP11/12	U_L46	Yes	395.80	538.88
	VP13/14	U_L47	Yes	1912.27	3286.98
	VP16 or ICP25	U_L48	Yes	1029.46	1587.92
	VP22	U_L49	Yes	1342.28	1289.80
	U_L50	U_L50	Yes	147.57	95.07
	U_L51	U_L51	Yes	141.66	175.12
	U_L55	U_L55	No	54.96	
	U_L56	U_L56	No	35.82	
	ICP4	R_S1	Yes	129.86	207.03
	ICP22	U_S1	Yes	4.62	30.32
	U_S2	U_S2	Yes	98.11	
	U_S3	U_S3	Yes	29.55	93.22
	U_S9	U_S9	Yes		6.29
	U_S10	U_S10	No	100.01	
	U_S11	U_S11	No	66.41	
Unknown	CIRC	circ	No		308.90
	U_L2	U_L2	Yes	13.77	18.48
	$U_L3.5$	$U_L3.5$	No		1335.08
	U_L15	U_L15	Yes		10.70
	U_L29	U_L29	Yes		13.30
	ICP6	U_L39	Yes	183.47	10.91
	ICP10	U_L40	Yes	30.61	28.85
	U_L42	U_L42	Yes		107.51
	ICP27	U_L54	Yes	4.97	17.14
	$U_S1.67$	$U_S1.67$	No		118.54

[a]Shown is a side-by-side comparison of BoHV-1 and HSV-1 virion compositions based on data presented in Tables 1 and 2 for HSV-1 and BoHV-1 homologues.

membrane. These observations suggest that capsid association with the INM does not regulate budding of the INM in BoHV-1-infected cells and that, as is known for HSV-1 and PRV, scission of the budded INM is an autonomous process that can occur efficiently in the absence of a capsid cargo (16).

In addition to capsidless budding at the INM, we were also able to identify surprisingly large numbers of capsidless light particles (L-particles) within the cyto-

TABLE 4 A subset of host cell proteins detected in extracellular HSV-1 and BoHV-1 virions[a]

Human Accession	Bovine Accession	Name	HSV-1 Protein score	BoHV-1 Protein score
P13645	A6QNZ7	Keratin, type I cytoskeletal 10	780.67	155.27
P13647	M0QVZ6	Keratin, type II cytoskeletal 5	377.81	244.26
P02533	F1MC11	Keratin, type I cytoskeletal 14	298.85	310.31
P07355	P04272	Annexin A2	221.45	647.32
P51149	P50397	Ras-related protein Rab-7a	181.43	205.69
P11142	P19120	Heat shock cognate 71 kDa protein	181.00	604.63
P04083	F1N650	Annexin A1	170.78	365.45
Q02413	G3N269	Desmoglein-1	153.29	35.15
P62140	P61585	Serine/threonine-protein phosphatase PP1-beta catalytic subu	134.36	240.18
P07737	P02584	Profilin-1	126.17	291.02
P62820	P62261	Ras-related protein Rab-1A	122.43	150.07
P61106	A3KN22	Ras-related protein Rab-14	106.28	162.61
P06733	F1MB08	Alpha-enolase	101.68	97.94
P62258	F1MW57	14-3-3 protein epsilon	100.28	158.88
Q15836	F1MTV5	Vesicle-associated membrane protein 3	98.28	141.65
P04075	A6QLL8	Fructose-bisphosphate aldolase A	96.20	77.44
P61019	A4FV54	Ras-related protein Rab-2A	90.11	101.41
P37802	G3X745	Transgelin-2	85.24	233.50
P63104	Q5E9E6	14-3-3 protein zeta/delta	84.93	181.68
P54920	Q3T0C6	Alpha-soluble NSF attachment protein	79.40	262.28
P22626	P15246	Heterogeneous nuclear ribonucleoproteins A2/B1	71.28	217.49
P14618	A5D984	Pyruvate kinase PKM	67.31	144.71
P61026	Q148J4	Ras-related protein Rab-10	65.51	76.86
P09211	P28801	Glutathione S-transferase P	64.76	33.14
P35052	F1MX83	Glypican-1	64.20	223.36
P13639	Q3SYU2	Elongation factor 2	63.85	91.30
Q8N1N4	A0JND2	Keratin, type II cytoskeletal 78	63.85	19.16
P27348	Q3T169	14-3-3 protein theta	56.32	105.60
Q15365	P37980	Poly(rC)-binding protein 1	51.25	51.74
Q13190	F1MIW8	Syntaxin-5	50.02	33.16

[a]Shown are host cell proteins identified based on a <1% FDR. The protein score reflects the number of peptides, abundance, and protein size to give a degree of confidence in protein identification. Data sets are shown in full in Tables S1 to S3 in the supplemental material. Accession numbers were acquired from the UniProt human and *Bos taurus* databases (https://www.uniprot.org/proteomes/UP000005640 and https://www.uniprot.org/proteomes/UP000009136).

plasm (Fig. 3C). These particles were of the same diameter as full virions, were wrapped in a double membrane, and contained electron-dense material that is likely to be tegument (Fig. 3C). Moreover, the extracellular population of released particles contained a high proportion of capsidless L-particles (Fig. 3D), which when measured for two strains of BoHV-1 amounted to around 50% of all released particles (Fig. 3E). In comparison, we found approximately 2% capsidless L-particles in similar electron micrographs of HSV-1-infected cells (not shown).

BoHV-1 particle assembly proceeds in the absence of DNA replication. Since both nuclear budding and particle egress can occur in the absence of a capsid cargo, we reasoned that, as for HSV-1 (24), both stages would be detectable in the absence of DNA replication. To examine this, BoHV-1 infection was perturbed by treatment with the nucleoside analogue arabinofuranosyl cytidine (AraC). AraC effectively blocked BoHV-1 genome replication as measured by semiquantitative PCR (Fig. 4A), while the late protein U_L47 (VP8) was expressed albeit at lower levels than in untreated cells (Fig. 4B). TEM analysis of AraC-treated infected cells revealed a variety of budding events at the inner nuclear membrane, including incomplete budding through the INM (Fig. 4C and D) as well as fully formed perinuclear vesicles (Fig. 4E). A small number of these vesicles contained B capsids (Fig. 4E, white arrowhead), but the majority of them were empty, confirming that INM budding proceeds even when prior steps of virus assembly have not taken place.

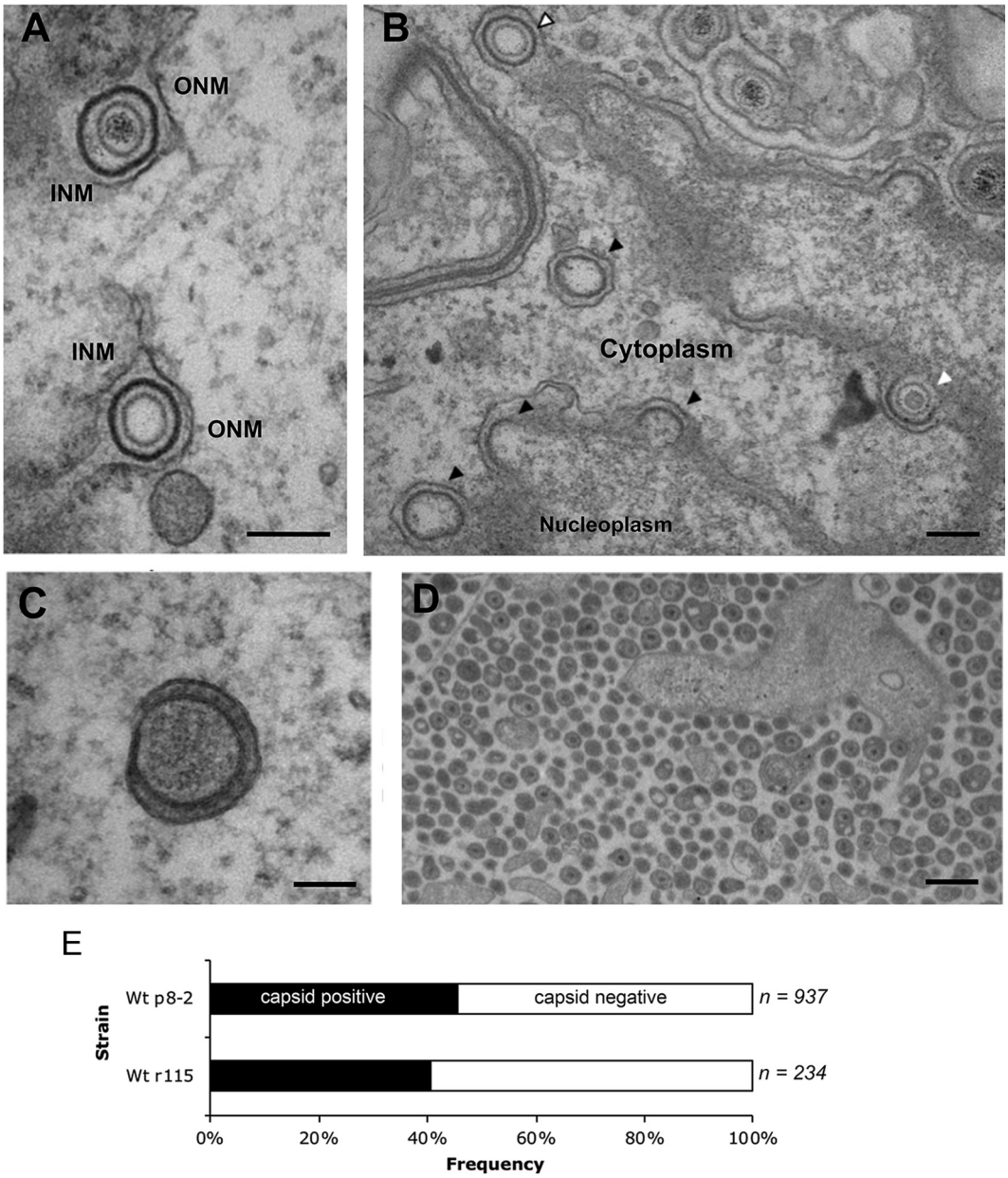

FIG 3 A variety of wrapping events occur in BoHV-1-infected cells. MDBK cells were infected at an MOI of 5 with BoHV-1 and fixed and processed for transmission electron microscopy at 12 hpi. (A and B) Representative sections of the nuclear envelope. In panel B, nuclear budding profiles that contain capsids resembling B capsids (white arrow) and A capsids (white arrow with black outline) or those occurring without a capsid (black arrows) are indicated. Bar = 200 nm. INM, inner nuclear membrane; ONM, outer nuclear membrane. (C) Fully wrapped capsidless L-particles were detected in the cytoplasm. Bar = 100 nm. (D) Multiple extracellular particles included full virions and capsidless L-particles. Bar = 500 nm. (E) Extracellular particles of MDBK cells infected with two strains of BoHV-1 were scored for the presence or absence of a capsid. Wt, wild type.

In addition to nuclear budding, cytoplasmic membranes that had a degree of curvature similar to that observed in infection of untreated cells were identified (Fig. 4F and G). Although capsids were not associated with these membranes, their curvature and size were such that capsids could be accommodated. Electron-dense material was seen to be associated with some of these endocytic membranes, which may represent assembling tegument (Fig. 4F and G, black arrows). Densely packed clusters of capsidless particles with consistent diameters were also noted outside the infected cells (Fig. 4H), and these particles had apparent glycoprotein spikes on their surface (Fig. 4I). These electron micrographs indicate that particle production continued efficiently in the absence

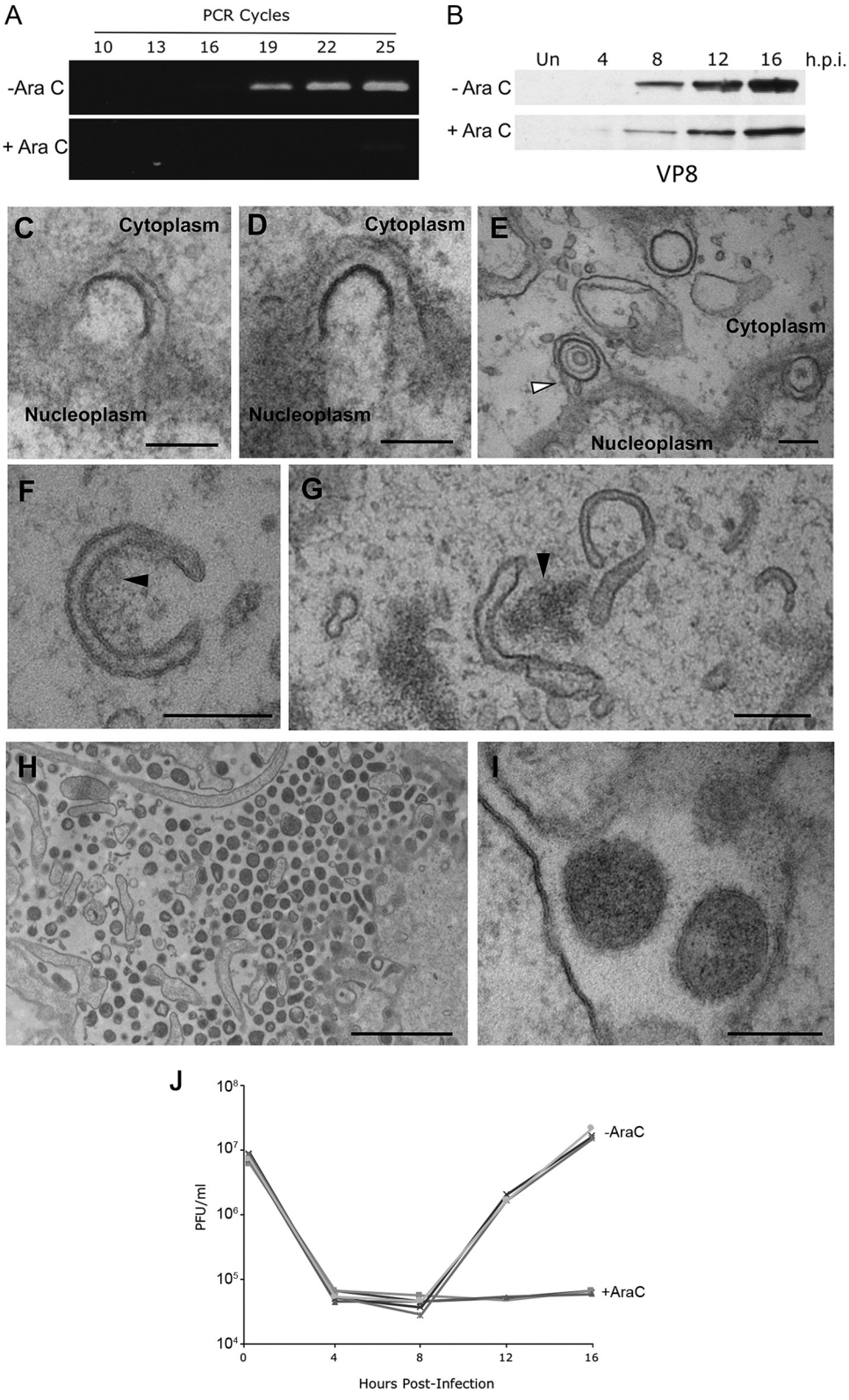

FIG 4 Inhibition of DNA replication with AraC does not arrest alternative wrapping events. (A and B) MDBK cells were infected at an MOI of 5 with BoHV-1 in the absence or presence of 100 μg/ml AraC. (A) The level of BoHV-1 genomic DNA was measured at 16 h by semiquantitative PCR using primers specific for U_L47. (B) Synthesis of the late VP8 protein was measured by Western blotting of samples harvested at the indicated times. Un, uninfected. (C to I) MDBK cells were infected at an MOI of 5 with BoHV-1 in the presence of 100 μg/ml AraC. Samples were fixed and processed at 16 h, before processing for transmission electron microscopy. (C and D) Incomplete budding through the INM in the direction of the perinuclear space. (E) Several sealed vesicles are shown in the perinuclear

(Continued on next page)

of BoHV-1 DNA replication, and we predict that these particles are L-particles enveloped via the normal envelopment route in the absence of capsid production. A one-step growth curve carried out in the absence or presence of AraC also confirmed that no infectious particles were produced under these conditions (Fig. 4J).

Proteomic composition of L-particles generated during BoHV-1 and HSV-1 infection. To characterize the relative composition of BoHV-1 L-particles in comparison to virions, the upper (light) and lower (virion) bands on a Ficoll gradient (Fig. 5A) were harvested by needle puncture through the side of the tube and analyzed by SDS-PAGE, followed by staining with Coomassie blue (Fig. 5B). As before, bands corresponding to the sizes expected for several characteristic virus proteins were identified, with a band corresponding to the major capsid protein (VP5) detectable in virions but barely detectable in L-particles, suggesting negligible contamination of this sample with virions. Many of the proteins were present at similar levels in both samples, but at least five proteins were identified as being differentially packaged into virions, as indicated by black dots (Fig. 5B). While several of these are likely to be capsid proteins, at least one of them, U_L36, is a known inner tegument protein. To compare the composition of L-particles to that of virions in greater detail, a duplex tandem mass tagging (TMT) system was used to label L-particle and virion samples, and mass spectrometry was used to identify and quantify the different proteins present in these samples (44). Initial analysis of the raw data indicated that, as expected, the L-particle/virion ratios of each virus glycoprotein were similar and ranged from 1 to 1.6 (Table 5). Therefore, to facilitate the subsequent analysis of the total data set, the light particle/virion ratios of all glycoproteins were averaged, and all light particle/virion ratios were normalized to this value. The results are summarized according to their predicted location in the envelope, tegument, or capsid (Fig. 5C), with total protein scores provided in Table 5. This shows that while envelope proteins were roughly equally abundant in the two populations, and the abundances of most of the proteins classified as capsid proteins were greatly reduced in L-particles, the BoHV-1 tegument proteins segregated into two groups: those that behaved like capsid proteins and were found mainly within virions and those that were equally as or more abundant within L-particles.

The ratios of individual proteins have been further grouped according to their predicted location within the virion and ranked according to the number of unique peptides identified for each of them (Fig. 5D). As also shown in Fig. 5C, the individual envelope proteins are tightly grouped around the normalization line (Fig. 5D). In contrast, the abundances of the capsid proteins U_L19, U_L25, U_L26, and U_L35 were greatly reduced in the L-particle samples (Fig. 5D). Interestingly, the U_L17 protein was the most abundant capsid protein in the BoHV-1 L-particles, in agreement with a previous study showing U_L17 as a component of both the tegument and capsid of HSV-1 (45). Among the tegument proteins, those that segregated with virions included the known inner tegument proteins U_L36 and U_L37 (Fig. 5D). Additionally, U_L48, U_L21, U_L16, and $U_L3.5$ proteins also appeared to be depleted from the L-particle samples. It should be noted that the results for those proteins to the right-hand side of each section of Fig. 5D (for example, the U_L6 capsid protein and BICP22 in the tegument) should be treated with caution because of their low protein score and number of unique peptides identified (Fig. 5D). Nonetheless, the high protein scores for the more abundant tegument proteins provide confidence in the analysis, and taken together, this would suggest that each of the inner tegument proteins that is predicted to link the virus capsid to the tegument in the virion is barely present within our L-particle

FIG 4 Legend (Continued)
space, with the arrow indicating a vesicle containing a B capsid. (F and G) Curved cytoplasmic tubules within the cytoplasm, frequently in association with electron-dense aggregates of material, indicated by the black arrows. (H and I) Extracellular space immediately adjacent to the plasma membrane, showing electron-dense particles, without a capsid cargo. Bars = 200 nm (C to G and I) and 2 μm (H). (J) MDBK cells were infected at an MOI of 5 with BoHV-1 in the absence (−AraC) or presence (+AraC) of 100 μg/ml AraC. Total virus was harvested at the indicated times and titrated on MDBK cells. Data from three biological replicates under each condition are shown.

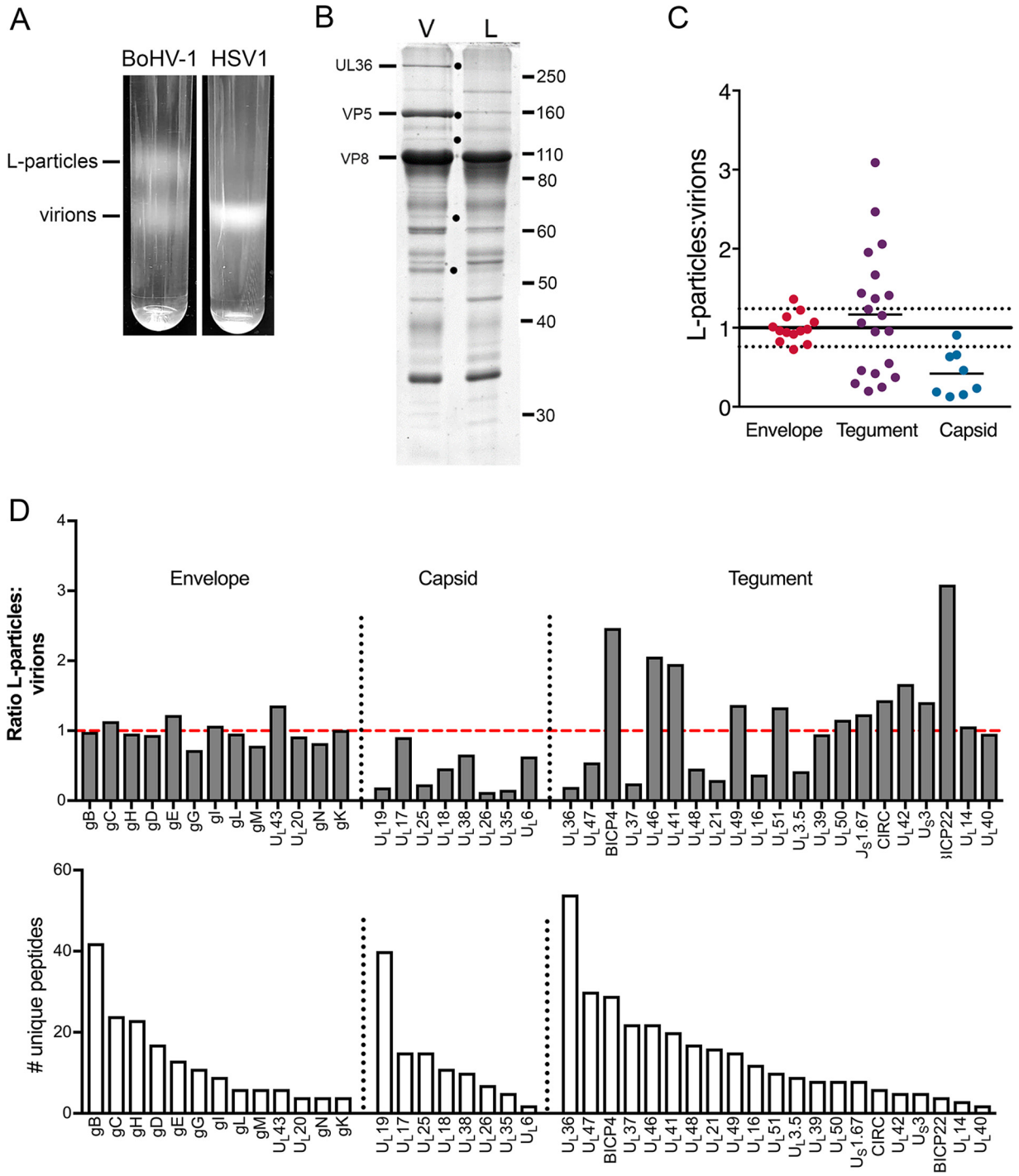

FIG 5 Quantitative proteomic comparison of the L-particles and virions produced during BoHV-1 infection. (A) Confluent monolayers of MDBK cells were infected with BoHV-1 strain P8-2, and HaCaT cells were infected with HSV-1 strain Sc16, both at a multiplicity of 0.02. At full cytopathic effect, the extracellular medium was harvested, and released particles were isolated on 5% to 15% Ficoll gradients. Representative Ficoll gradients of BoHV-1 and HSV-1 particle preparations isolated at the same time are shown. (B) Equal amounts of the virion (V) and L-particle (L) bands of BoHV-1 were separated by 10% SDS-PAGE and stained with Coomassie blue. Black dots denote protein bands present in virions but not L-particles. Size markers are shown in kilodaltons. (C) The BoHV-1 virion and L-particle samples were subjected to TMT labeling and analyzed by mass spectrometry. Shown is a summary of the normalized ratios of virus proteins detected in BoHV-1 L-particles to virions, grouped according to their predicted location within the virion. The normalization line represents the average of all glycoprotein ratios, with 1 standard deviation on either side represented by dotted lines. (D) Ratio of individual virus proteins in BoHV-1 L-particles compared to virions (top), in order of the number of unique peptides detected (bottom). The dashed red line is the glycoprotein normalization line.

TABLE 5 Results of TMT proteomic analysis of BoHV-1 L-particles and virions[a]

Accession	Name	Protein score	Coverage	# Unique Peptides	L-particle to virion ratio	Variability
P10230	VP11/12	51.38	32.31	19	10.378	20.6
P04487	U_S11	4.64	15.53	2	7.352	6.6
P10234	UL50	6.95	10.24	3	4.125	2.5
P10211	gB	19.25	9.40	8	2.631	9.1
P10235	U_L51	3.99	12.70	2	2.454	21.1
P10229	UL45	13.68	22.09	3	2.206	8.5
Q69091	gD	37.07	31.98	10	2.172	13.7
P10228	gC	35.50	17.42	6	2.002	8.2
P08543	ICP6	2.00	2.37	2	1.861	311.3
P10225	VHS	10.60	12.07	5	1.818	16.2
P10201	U_L17	7.26	8.25	3	1.627	59.8
P10185	gL	8.68	21.43	4	1.611	12.4
P06477	gH	45.90	26.73	16	1.527	12.8
P08392	ICP4	4.43	2.93	3	1.451	0.2
P06487	gI	15.49	36.15	6	1.431	26.9
P04488	gE	22.38	27.82	11	1.427	18.4
P04288	gM	12.83	18.18	5	1.398	8.0
P10233	VP22	67.42	68.44	15	1.356	8.3
P04289	U_L11	15.02	20.83	2	1.354	3.8
P10231	VP13/14	111.60	71.43	35	1.249	13.8
P10220	U_L36	117.91	21.71	49	1.201	13.7
P10205	U_L21	41.83	36.45	16	1.186	13.3
P10200	U_L16	9.47	27.61	7	1.158	6.9
P10221	U_L37	46.98	27.25	19	1.148	10.5
P06492	VP16	42.30	35.10	11	1.068	11.0
P10202	VP23	5.77	12.26	3	1.012	5.5
P10209	U_L25	18.42	15.52	7	0.645	27.1
P10210	VP24	11.93	8.82	5	0.306	53.6
P06491	VP5	19.66	6.62	7	0.273	66.5
P32888	VP19c	12.31	12.90	5	0.268	35.8

[a]BoHV-1 proteins were identified based on a <1% FDR, with the L-particle-to-virion ratio for each protein shown.

preparation. In short, BoHV-1 L-particles appear to be assembled without the inner tegument-capsid-interacting proteins.

Although we have found that HSV-1 L-particles were much less abundant in extracellular purified particle populations from HaCaT cells than BoHV-1 from MDBK cells (Fig. 5A), we harvested the equivalent regions of the HSV-1 gradient as we had for the BoHV-1 gradient, which enabled us to isolate a small number of HSV-1 L-particles for proteomic analysis as described above for BoHV-1. In contrast to BoHV-1, most HSV-1 tegument proteins appeared to be largely equally abundant in virions and L-particles (Fig. 6A and B; total protein scores are provided in Table 6). In particular, further analysis revealed that unlike BoHV-1, the inner tegument proteins of HSV-1 were abundant in L-particles (Fig. 6A), as has been shown by others (22). Interestingly, U_L46 (VP11/12) and U_S11 were enriched around >6-fold and 4-fold, respectively, in L-particles, and U_L50 was enriched to a lesser extent, >2-fold (Fig. 6A).

Because the HSV-1 L-particles were difficult to isolate, and to ensure that this enhanced incorporation was reproducible, a second isolation of HSV-1 virions and L-particles was carried out and analyzed by TMT mass spectrometry. This confirmed that the tegument proteins were all approximately equally abundant in HSV-1 L-particles and virions, again with the exception of U_L46 and U_S11 (Fig. 6C). However, on this occasion, U_L50 was undetectable in the samples, while ICP0 was detected in the second but not the first preparation. This showed that, as for BoHV-1, variability in the

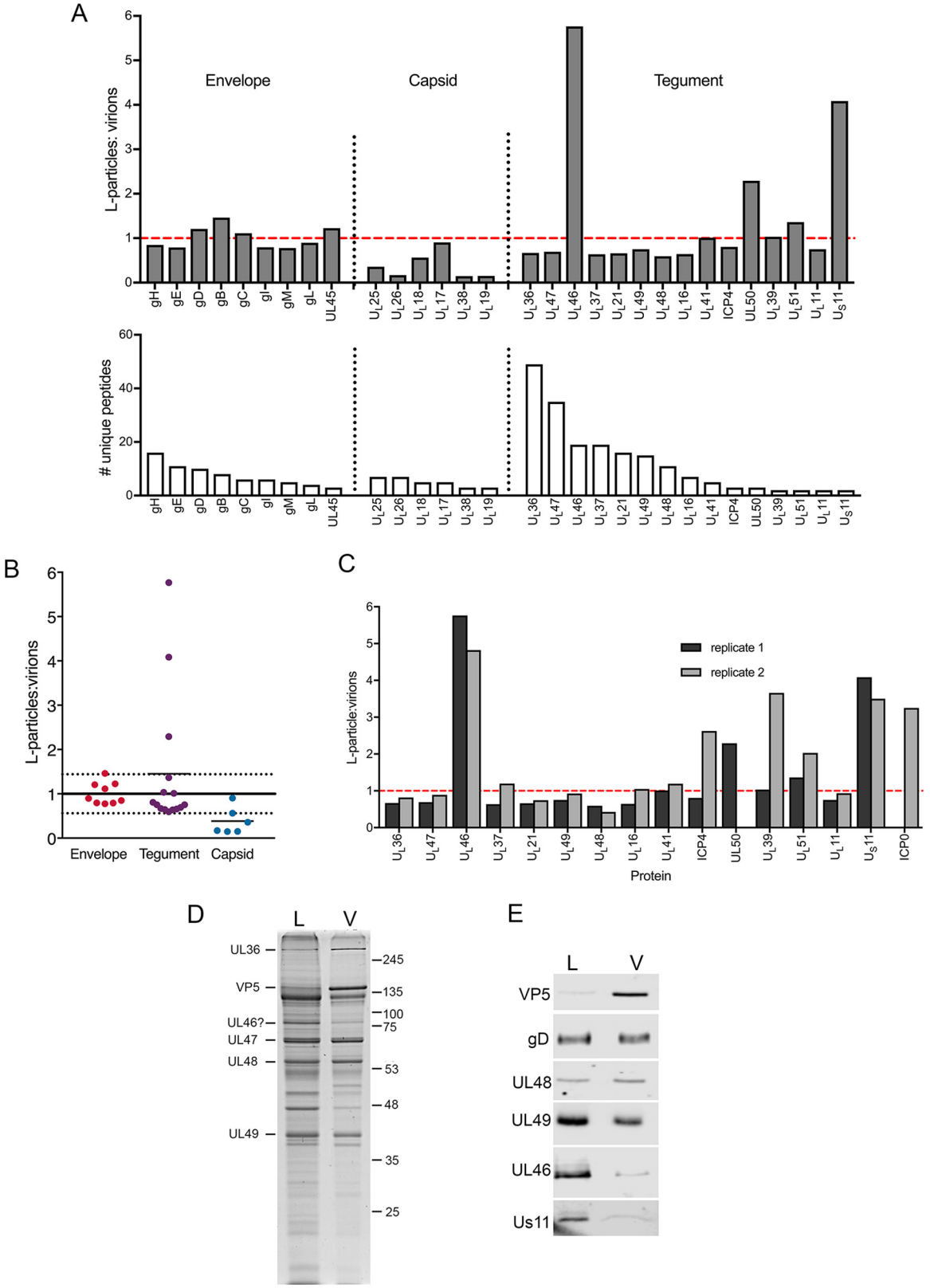

FIG 6 Quantitative proteomic comparison of the L-particles and virions produced in HSV-1 infection. (A) A Ficoll gradient for HSV-1 strain Sc16 similar to that shown in Fig. 5A was harvested for virions and L-particles as for BoHV-1 and analyzed by tandem mass tag labeling mass spectrometry as for BoHV-1. The results are presented as the ratio of the number of individual virus proteins in HSV-1 L-particles to virions (top), in order of the number of unique peptides detected (bottom). The dashed red line is the glycoprotein normalization line. (B) Summary of the normalized ratios of virus proteins detected in HSV-1 L-particles to virions, grouped according to their predicted

(Continued on next page)

content of proteins detected by low peptide numbers could not provide confidence in the results to the extreme right-hand side of the graph. To further validate these proteomic results, approximately equivalent numbers of a third preparation of HSV-1 L-particles and virions, as judged by Coomassie blue staining (Fig. 6D), were analyzed by Western blotting for the presence of a range of virus proteins, as indicated (Fig. 6E). As predicted from the mass spectrometry analysis, gD, VP22, and VP16 were similarly abundant in L-particles and virions, while the major capsid protein VP5 encoded by U_L19 was enriched in the virion sample. In contrast, both U_L46 and U_S11 were enriched in the L-particle sample, confirming the results of the mass spectrometry analysis (Fig. 6E). Of note, Western blotting of virions and L-particles for ICP34.5 failed to detect this protein despite a strong positive blot from infected cell lysates (data not shown). While we cannot exclude the possibility that the differences found in L-particle content between BoHV-1 and HSV1 were a consequence of the cell types used to purify the particles, these data highlight the fact that there are virus-specific variations in the makeup of noninfectious L-particles.

DISCUSSION

In this study, we have extended our previous studies on HSV-1 morphogenesis (17) to provide evidence that BoHV-1 may follow a pathway similar to that of HSV-1. In ultrastructural studies, BoHV-1 wrapping events were similar to those previously found for HSV-1, with capsids associating with curved tubules which were positive for HRP that had been taken up by fluid-phase endocytosis. Given the growing evidence for the role of endocytosis at the molecular and ultrastructural levels for a range of herpesviruses (17, 20, 46–48), we propose that this model, which requires virus glycoproteins to first traffic to the plasma membrane before being retrieved into the endocytic membranes, may represent a unifying model of alphaherpesvirus envelopment. Many of the endocytic tubules found in the cytoplasm of BoHV-1-infected cells exhibited a reproducible membrane curvature and contained budded domains, with the diameter, density, and structure bearing strong similarities to those of endocytic clathrin coats previously reported in uninfected cells (49). The presence of clathrin-like coats has also been reported in cryo-electron microscopy (EM)-based studies of HSV-1 envelopment (17, 26). Similarly, our studies have shown that BoHV-1 exhibits the same primary envelopment profiles, budding at the INM and within the perinuclear space, that have been identified for several other herpesviruses, including HSV-1 and PRV (13). However, compared to our previous results with HSV-1, these profiles were numerous and readily detectable in BoHV-1-infected cells, indicating that these events occur either more frequently or more slowly than in HSV-1. In addition to ultrastructural studies, we have also carried out the first side-by-side proteomic study of HSV-1 and BoHV-1 virions, both of which have been previously characterized independently by mass spectrometry (8, 10). In general, our results are in agreement with those previous studies, despite differences in strains of virus and cell lines used to produce the extracellular virions and confirm that the complements of virus-encoded proteins packaged into virions are similar for both viruses. In the case of HSV-1, we confirmed the absence of glycoproteins U_L43, gJ, and gN but were able to detect two glycoproteins, gK and U_L45, that had not been previously identified in its proteome. In BoHV-1, we detected 20 more virion proteins than in the previous study, including several proteins that were also present in HSV-1 virions. Glycoprotein G, encoded by U_S4, was found to be highly abundant in BoHV-1 virions but hardly detectable in HSV-1 virions. Nevertheless, it is important to consider than many of these constituents had mass spectrometry scores lower than

FIG 6 Legend (Continued)
location within the virion. The normalization line represents the average of all glycoprotein ratios, with 1 standard deviation on either side represented by dotted lines. (C) Comparative ratios of individual tegument proteins between two independent TMT labeling analyses. (D and E) Approximately equivalent amounts of Sc16 virions (V) and L-particles (L) were subjected to SDS-PAGE on a 10% polyacrylamide gel followed by Coomassie blue staining (D) or Western blotting (E) for the indicated virus proteins. Approximately equivalent numbers of particles were loaded by equating gD and U_L48 by Western blotting. Molecular weight markers are shown in kilodaltons.

TABLE 6 Results of TMT proteomic analysis of HSV-1 L-particles and virions[a]

Accession	Name	Protein score	Coverage	# Unique Peptides	L-particle to virion ratio	Variability in ratio
A0A089N2D8	BICP22	4.47	13.58	4	4.169	15.1
A0A089N2E7	BICP4	87.12	29.87	29	3.332	51.9
A0A089N3R8	VP11/12	112.24	34.33	22	2.780	18.0
A0A089N2A0	VHS	52.12	49.46	20	2.638	13.7
A0A089N629	U_L42	4.65	15.44	5	2.251	14.6
A0A089N3R1	CIRC	28.24	32.52	6	1.939	10.3
A0A089PGK8	U_S3	13.99	22.58	5	1.903	15.6
A0A089PGG2	VP22	86.58	68.99	15	1.847	5.8
A0A089PGG6	U_L43	16.90	17.46	6	1.839	7.3
A0A089N291	U_L51	24.31	47.74	10	1.799	8.3
A0A089N3W0	$U_S1.67$	26.84	50.62	8	1.666	13.0
A0A089N810	gE	53.96	34.43	13	1.652	11.0
A0A089N3R5	U_L50	16.80	39.08	8	1.561	31.7
A0A089N7W5	gC	407.14	39.57	24	1.536	9.2
A0A089N3W4	gI	47.11	30.63	9	1.446	15.7
A0A089PGJ2	U_L14	10.88	21.88	3	1.431	4.5
A0A089PGF7	gK	16.83	23.37	4	1.364	10.7
A0A089N646	gB	226.55	43.30	42	1.326	10.5
A0A089N804	gL	17.86	44.94	6	1.297	12.9
A0A089N2B7	gH	102.36	36.58	23	1.295	9.7
A0A089N3S3	U_L40	5.08	8.25	2	1.292	14.3
A0A089N7X0	U_L39	14.20	13.60	8	1.283	27.3
A0A089N2E3	gD	85.54	39.09	17	1.268	9.0
A0A089N7Y8	U_L20	14.78	31.17	4	1.239	9.8
A0A089N3U4	U_L17	33.21	24.18	15	1.225	5.4
A0A089N7V8	gN	18.49	26.04	4	1.112	13.1
A0A089N7Z6	gM	89.87	14.84	6	1.062	9.0
A0A089N688	gG	103.40	30.41	11	0.977	12.5
A0A089PGH0	U_L38	39.10	31.16	10	0.888	11.0
A0A089N3V3	U_L6	4.29	4.36	2	0.853	115.2
A0A089N295	VP13/14	441.07	53.98	30	0.740	12.7
A0A089N657	U_L18	21.77	35.13	11	0.621	18.1
A0A089N623	VP16	85.16	43.39	17	0.620	19.3
A0A089N675	$U_L3.5$	83.64	62.70	9	0.567	21.2
A0A089N7Z2	U_L16	26.64	41.11	12	0.503	27.5
A0A089N3U0	U_L21	57.18	35.29	16	0.398	48.2
A0A089N634	U_L37	35.90	26.31	22	0.334	39.0
A0A089N7Y3	U_L25	40.01	31.77	15	0.316	43.7
A0A089N2A4	U_L36	121.19	24.21	54	0.266	62.8
A0A089PGI7	U_L19	88.38	37.58	40	0.253	29.5
A0A089N3S8	U_L35	34.71	54.03	5	0.207	37.8
A0A089N3T6	U_L26	13.65	16.40	7	0.170	86.9

[a]Shown are HSV-1 proteins identified based on a <1% FDR, with the L-particle-to-virion ratio for each protein shown.

that for the portal protein U_L6, which is known to be present in just 12 copies in each virion. While protein score is not a direct readout of protein abundance in the sample, it is an indication that these proteins were difficult to detect in the virion samples. There are a number of potential explanations for this: (i) they are present in very low copy numbers in each particle, (ii) they are present in vastly variable numbers between particles, or (iii) they are simply contaminants from the cell extract that had been detected by the increased sensitivity of mass spectrometry. For example, the U_L34 component of the NEC was detected at very low levels in particles from both viruses,

but given its role at the nuclear membrane, it may not be expected to be incorporated into the mature particle. In addition, while the presence of glycoprotein K was convincing in both viruses, the level of its partner glycoprotein U_L20 was extremely low (50, 51). Finally, despite the increased sensitivity of our mass spectrometry analysis, we failed to identify either ICP34.5 or U_S9 in HSV-1 virions, both of which had been detected by only a single peptide in the previous proteomic study on HSV-1 (10).

We found that in BoHV-1-infected cells, the capsidless envelopment events occurred with great efficiency. As a consequence, we were able to isolate released L-particles and compare their composition to that of BoHV-1 virions by mass spectrometry. Intriguingly, this revealed that the BoHV-1 L-particles, although not retrieved as a completely homogeneous population free of contaminating virions, were depleted for U_L36, U_L37, and U_L48, essential tegument proteins that link the capsid to the tegument/envelope structure of alphaherpesviruses (27). Three other tegument proteins, U_L21, U_L16, and $U_L3.5$, were also notable for being depleted from the BoHV-1 L-particles. U_L21 has been shown to be involved in nuclear egress of HSV-1 and HSV-2 capsids (52, 53), suggesting a potential role in bridging the capsid to the envelope. Likewise, U_L16 has been shown to be required for the egress of HSV-2 capsids from the nucleus (54) but has not been designated this role in HSV-1, where deletion of U_L16 has a limited effect on virus replication (55). Interestingly, a recent study from the Banfield group has shown that HSV-1 U_L16 rescues the nuclear egress defect in the HSV-2 knockout virus, suggesting that HSV-1 has another factor absent from HSV-2 that fulfils this role in the absence of U_L16 (56). In light of this, it is important to note that as for HSV-2, BoHV-1 U_L16 is essential for BoHV-1 replication (57). Finally, the $U_L3.5$ protein is not present in HSV-1, but for BoHV-1, it has been shown to interact with U_L48 (58), an interaction which might also place it within the inner tegument. Taken together with the high abundance of these particles, and the fact that they were efficiently produced in the absence of DNA replication, we propose that BoHV-1 L-particles lack the inner tegument, represent enveloped outer tegument proteins, and are produced in an event that is autonomous and entirely independent of steps prior to final wrapping in the assembly pathway. In support of this, studies on other viruses have shown that L-particles are produced in the absence of DNA replication, DNA packaging, or delivery of capsids to the cytoplasm (24, 59, 60), indicating that at least some of the proteins that make up L-particles are sufficient to direct the envelopment process (22). Moreover, the fact that the complements of outer tegument proteins are similar in full virions and L-particles would suggest that they share the same morphogenesis and release pathway, in agreement with data from other studies on PRV (61).

In contrast, in our hands, HSV-1 L-particles were released from human keratinocytes in much lower numbers. While we recognize that the level of L-particle production appears to be cell type dependent for HSV-1 (62), our result in HaCaT cells is in agreement with our previous experience of isolating HSV-1 particles from both BHK21 and Vero cells, where we consistently recover large numbers of infectious virions but few observable L-particles, as illustrated in Fig. 5A. Unfortunately, it is not possible to compare the two viruses in the same cell line, as BoHV-1 is restricted in its host range, while, consistent with previous studies (63, 64), we have been unable to isolate HSV-1 particles from MDBK cells. Nonetheless, two replicate preparations of HSV-1 L-particles from HaCaT cells revealed that unlike BoHV-1, the inner tegument proteins were incorporated into HSV-1 L-particles to approximately the same level as in virions. Interestingly, the U_L46 tegument protein was reproducibly enhanced around 5-fold in HSV-1 L-particles compared to virions, a feature that may provide clues to the HSV-1 L-particle assembly-and-trafficking pathway. In relation to this, the biological significance of L-particles remains unknown, but as suggested by others (65), it is tempting to speculate that BoHV-1 L-particles in particular could deliver large amounts of outer tegument proteins to uninfected cells ahead of or as an enhancement to infecting virus. As it is now becoming clear that many of these proteins may have roles in counteracting cellular antiviral responses (66), the initial infected cell could potentially send out a wave of these particles to either deliver proteins that can fight a preexisting antiviral

state set up by interferons or prevent responses induced by subsequent incoming infection. It is therefore interesting to note that HSV-1 U_L46 has recently been assigned a role in evading the STING-cGAS DNA-sensing pathway (67), while BoHV-1 U_L47 is proposed to inhibit interferon signaling by binding to STAT1 (68).

In summary, the abundance and tractability of BoHV-1 L-particle production make this system particularly attractive to further our understanding of virus morphogenesis and the role of tegument proteins. Moreover, the potential therapeutic application of these noninfectious particles, such as vaccine development or the packaging and delivery of heterologous overexpressed proteins, is a much more realistic prospect given a system that is exquisitely designed to produce these particles efficiently and in large amounts.

MATERIALS AND METHODS

Cells and viruses. Vero cells were cultured in Dulbecco's modified Eagle medium (DMEM) supplemented with 10% newborn calf serum (NCS) and 50 U/ml penicillin-streptomycin. HaCaT and MDBK cells were cultured in DMEM supplemented with 10% fetal bovine serum and 50 U/ml penicillin-streptomycin. HSV-1 strain Sc16 was routinely propagated and titrated in Vero cells in DMEM supplemented with 2% NCS and 50 U/ml penicillin-streptomycin. BoHV-1 strains P8-2 and r115 were routinely propagated and titrated in MDBK cells in DMEM supplemented with 2% NCS and 50 U/ml penicillin-streptomycin.

Isolation of extracellular virus particles. For mass spectrometry-based studies, released HSV-1 and BoHV-1 virions and L-particles were gradient purified as described previously (69). Briefly, 10 175-cm^2 flasks of confluent MDBK or HaCaT cells (approximately 6×10^8 cells in total) were infected with BoHV-1 (strain P8-2) or HSV-1 (strain Sc16) at a multiplicity of 0.02. Once cytopathic effect was advanced (3 to 4 days postinfection), the extracellular medium was collected and centrifuged at 3,000 rpm for 30 min at 4°C in a fixed-angle rotor to remove cell debris. Virus particles were then pelleted from the cleared supernatant at 9,000 rpm for 90 min at 4°C. The particle pellet was resuspended in 0.5 ml phosphate-buffered saline (PBS) and carefully layered onto a preformed 11-ml 5% to 15% (wt/vol) Ficoll gradient in a 13.2-ml thin-wall polyallomer ultracentrifuge tube (Beckman Coulter). Gradients were centrifuged at 12,000 rpm for 2 h at 4°C in an SW41 Ti swinging-bucket rotor in a Sorvall Discovery SE ultracentrifuge. Light and heavy bands were harvested by needle puncture through the side of the tube with a 19-gauge hypodermic needle in a volume of <1 ml, diluted in 10 ml PBS, and pelleted at 25,000 rpm for 1 h at 4°C using the same rotor and ultracentrifuge. The pellets were resuspended in a suitable volume of PBS and stored at −80°C.

SDS-PAGE and Western blotting. Virus particle samples were separated by 9 or 10% SDS-PAGE and stained with Coomassie blue or transferred to nitrocellulose membranes before Western blotting. The following primary antibodies were used for Western blots and kindly provided: mouse anti-gD (LP14), from Tony Minson (University of Cambridge); mouse anti-VP16 (LP1), from Colin Crump (University of Cambridge); rabbit anti-U_L46, from Richard Courtney (Pennsylvania State University); rabbit anti-U_S11, from Ian Mohr (New York University); and mouse anti-VP5 (HA-018; Virusys). Our rabbit VP22-specific antibody (AGV031) has been described previously (70, 71). Goat anti-mouse IRDye 680RD and goat anti-rabbit IRDye 800CW (Li-Cor Biosciences) secondary antibodies were used as appropriate, before blots were imaged using an Odyssey CLx imaging system (Li-Cor Biosciences).

Conventional proteomic analysis of BoHV-1 and HSV-1 virions. BoHV-1 or HSV-1 virion samples were separated by SDS-PAGE, the gel lane was cut into three slices, and each slice was subjected to in-gel tryptic digestion using a DigestPro automated digestion unit (Intavis). The resulting peptides were fractionated using a nano-HPLC system with an LTQ-Orbitrap Velos mass spectrometer (ThermoFisher Scientific).

TMT proteomic analysis of BoHV-1 and HSV-1 L-particles and virions. A total of 100 μg of protein was digested with 2.5 μg trypsin overnight at 37°C and labeled with tandem mass tag (TMT) sixplex reagents according to the manufacturer's protocol (ThermoFisher Scientific). The virion and L-particle samples were then pooled, evaporated to dryness, resuspended in 5% (vol/vol) formic acid, and then desalted using Sep-Pak cartridges according to the manufacturer's instructions (Waters). The eluent from the Sep-Pak cartridge was evaporated to dryness and resuspended in 1% (vol/vol) formic acid before analysis by the nano-HPLC system with an Orbitrap Fusion Tribrid mass spectrometer (ThermoFisher Scientific).

Nano-HPLC mass spectrometry. Samples were fractionated using an Ultimate 3000 nano-HPLC system. In brief, peptides in 1% (vol/vol) formic acid were injected onto an Acclaim PepMap C_{18} nano-trap column (ThermoFisher Scientific). After washing with 0.5% (vol/vol) acetonitrile–0.1% (vol/vol) formic acid, peptides were resolved on a 250-mm by 75-μm Acclaim PepMap C_{18} reverse-phase analytical column (ThermoFisher Scientific) over a 150-min organic gradient, using seven gradient samples for conventional samples (1 to 6% solvent B [aqueous 80% {vol/vol} acetonitrile in 0.1% {vol/vol} formic acid] over 1 min, 6 to 15% solvent B over 58 min, 15 to 32% solvent B over 58 min, 32 to 40% solvent B over 5 min, and 40 to 90% solvent B for 6 min, which was then reduced to 1% solvent B over 1 min) or six gradient segments for TMT-labeled samples (5 to 9% solvent B over 2 min, 9 to 25% solvent B over 94 min, 25 to 60% solvent B over 23 min, and 60 to 90% solvent B over 5 min, which was held at 90% solvent B for 5 min and then reduced to 1% solvent B over 2 min), with a flow rate of 300 nl min^{-1}. Peptides were

ionized by nano-electrospray ionization at 2.0 or 2.1 kV using a stainless steel emitter with an internal diameter of 30 μm (ThermoFisher Scientific) and a capillary temperature of 275°C.

For conventional proteomics, tandem mass spectra were acquired using an LTQ-Orbitrap Velos mass spectrometer controlled by Xcalibur 2.1 software (ThermoFisher Scientific) and operated in the data-dependent acquisition mode. The Orbitrap was set to analyze the survey scans at a 60,000 resolution (at *m/z* 400) in the mass range *m/z* 300 to 2,000, and the top 20 multiply charged ions in each duty cycle were selected for tandem mass spectrometry (MS/MS) in the LTQ linear ion trap. Charge-state filtering, where unassigned precursor ions were not selected for fragmentation, and dynamic exclusion (repeat count, 1; repeat duration, 30 s; exclusion list size, 500) were used. Fragmentation conditions in the LTQ instrument were as follows: normalized collision energy of 40%, activation *q* of 0.25, activation time of 10 ms, and minimum ion selection intensity of 500 counts.

For TMT-labeled samples, all spectra were acquired by using an Orbitrap Fusion Tribrid mass spectrometer controlled by Xcalibur 2.0 software (ThermoFisher Scientific) and operated in the data-dependent acquisition mode using an SPS-MS3 workflow. FTMS1 spectra were collected at a resolution of 120,000, with an automatic gain control target of 400,000 and a maximum injection time of 100 ms. Precursors were filtered with an intensity range from 5,000 to 1×10^{20}, according to charge state (to include charge states 2 to 6), and with monoisotopic precursor selection. Previously interrogated precursors were excluded using a dynamic window (60 s $\pm$ 10 ppm). The MS2 precursors were isolated with a quadrupole mass filter set to a width of 1.2 *m/z*. ITMS2 spectra were collected with an AGC target of 10,000, a maximum injection time of 70 ms, and CID collision energy of 35%.

For FTMS3 analysis, the Orbitrap was operated at a 30,000 resolution with an AGC target of 50,000 and a maximum injection time of 105 ms. Precursors were fragmented by high-energy collision dissociation at a normalized collision energy of 55% to measure maximal TMT reporter ion yield. Synchronous precursor selection was enabled to include up to five MS2 fragment ions in the FTMS3 scan.

Proteomic data analysis. The raw data files were processed and quantified using Proteome Discoverer software v1.4 (ThermoFisher Scientific). The data were searched against either the UniProt human database (downloaded on 18 April 2016; 134,169 entries) and the UniProt human herpesvirus 1 (strain 17) database (downloaded on 11 April 2016; 73 entries) or the UniProt *Bos taurus* database (downloaded on 21 October 2016; 31,855 entries) and the UniProt bovine herpesvirus 1 (strain K22) database (downloaded on 21 October 2016; 69 entries) as appropriate. All searches were performed using the SEQUEST algorithm. The peptide precursor mass tolerance was set at 10 ppm, and the MS/MS tolerance was set at 0.8 or 0.6 Da. Search criteria included oxidation of methionine (+15.9949) as a variable modification and carbamidomethylation of cysteine (+57.0214) and the addition of the TMT mass tag (+229.163) to peptide N termini and lysine as fixed modifications. Searches were performed with full tryptic digestion, and a maximum of one missed cleavage was allowed. The reverse database search option was enabled, and all peptide data were filtered to satisfy a false discovery rate (FDR) of 5% or 1%.

Transmission electron microscopy. To prepare samples for electron microscopy, cells were grown to confluence overnight before infection with virus. When infection was carried out in the presence of AraC, all infection, washing, and incubation steps were performed in the presence of 100 ng/ml AraC. Horseradish peroxidase (HRP) labeling was performed as previously described (17), by incubating cells with 10 mg/ml HRP for 30 min prior to fixation. After fixation, samples were washed and stained with a metal-enhanced 3,3′-diaminobenzidine (DAB) substrate kit (ThermoFisher Scientific). The samples for electron microscopy were fixed and processed as previously described (72).

SUPPLEMENTAL MATERIAL

Supplemental material for this article may be found at https://doi.org/10.1128/JVI.01259-18.

SUPPLEMENTAL FILE 1, XLSX file, 0.1 MB.

ACKNOWLEDGMENTS

We thank Kate Heesom, University of Bristol, for conducting the mass spectrometry analyses. We also thank Tony Minson, Colin Crump, Richard Courtney, and Ian Mohr for antibodies used in this study.

This work was funded by the UK Medical Research Council (grant reference numbers G0601605 to G.E. at Imperial College London and MR/M020061/1 to G.E. at the University of Surrey). B.B. was funded by an MRC Ph.D. studentship, Imperial College London.

REFERENCES

1. Looker KJ, Magaret AS, May MT, Turner KME, Vickerman P, Newman LM, Gottlieb SL. 2017. First estimates of the global and regional incidence of neonatal herpes infection. Lancet Glob Health 5:e300–e309. https://doi.org/10.1016/S2214-109X(16)30362-X.

2. Looker KJ, Magaret AS, May MT, Turner KME, Vickerman P, Gottlieb SL, Newman LM. 2015. Global and regional estimates of prevalent and incident herpes simplex virus type 1 infections in 2012. PLoS One 10:e0140765. https://doi.org/10.1371/journal.pone.0140765.

3. Statham JME, Randall LV, Archer SC. 2015. Reduction in daily milk yield associated with subclinical bovine herpesvirus 1 infection. Vet Rec 177:339. https://doi.org/10.1136/vr.103105.
4. Bennett R. 2003. The 'direct costs' of livestock disease: the development of a system of models for the analysis of 30 endemic livestock diseases in Great Britain. J Agric Econ 54:55–71. https://doi.org/10.1111/j.1477-9552.2003.tb00048.x.
5. Muylkens B, Thiry J, Kirten P, Schynts F, Thiry E. 2007. Bovine herpesvirus 1 infection and infectious bovine rhinotracheitis. Vet Res 38:181–209. https://doi.org/10.1051/vetres:2006059.
6. Steiner I. 2013. Herpes virus infection of the peripheral nervous system. Handb Clin Neurol 115:543–558. https://doi.org/10.1016/B978-0-444-52902-2.00031-X.
7. Vlček Č, Beneš V, Lu Z, Kutish GF, Pačes V, Rock D, Letchworth GJ, Schwyzer M. 1995. Nucleotide sequence analysis of a 30-kb region of the bovine herpesvirus 1 genome which exhibits a colinear gene arrangement with the UL21 to UL4 genes of herpes simplex virus. Virology 210:100–108. https://doi.org/10.1006/viro.1995.1321.
8. Barber K, Daugherty H, Ander S, Jefferson V, Shack L, Pechan T, Nanduri B, Meyer F. 2017. Protein composition of the bovine herpesvirus 1.1 virion. Vet Sci 4:E11. https://doi.org/10.3390/vetsci4010011.
9. Mettenleiter TC. 2006. Intriguing interplay between viral proteins during herpesvirus assembly or: the herpesvirus assembly puzzle. Vet Microbiol 113:163–169. https://doi.org/10.1016/j.vetmic.2005.11.040.
10. Loret S, Guay G, Lippe R. 2008. Comprehensive characterization of extracellular herpes simplex virus type 1 virions. J Virol 82:8605–8618. https://doi.org/10.1128/JVI.00904-08.
11. Mettenleiter TC, Klupp BG, Granzow H. 2006. Herpesvirus assembly: a tale of two membranes. Curr Opin Microbiol 9:423–429. https://doi.org/10.1016/j.mib.2006.06.013.
12. Johnson DC, Baines JD. 2011. Herpesviruses remodel host membranes for virus egress. Nat Rev Microbiol 9:382–394. https://doi.org/10.1038/nrmicro2559.
13. Granzow H, Klupp BG, Fuchs W, Veits J, Osterrieder N, Mettenleiter TC. 2001. Egress of alphaherpesviruses: comparative ultrastructural study. J Virol 75:3675–3684. https://doi.org/10.1128/JVI.75.8.3675-3684.2001.
14. Fuchs W, Klupp BG, Granzow H, Osterrieder N, Mettenleiter TC. 2002. The interacting UL31 and UL34 gene products of pseudorabies virus are involved in egress from the host-cell nucleus and represent components of primary enveloped but not mature virions. J Virol 76:364–378. https://doi.org/10.1128/JVI.76.1.364-378.2002.
15. Bigalke JM, Heuser T, Nicastro D, Heldwein EE. 2014. Membrane deformation and scission by the HSV-1 nuclear egress complex. Nat Commun 5:4131. https://doi.org/10.1038/ncomms5131.
16. Klupp BG, Granzow H, Fuchs W, Keil GM, Finke S, Mettenleiter TC. 2007. Vesicle formation from the nuclear membrane is induced by coexpression of two conserved herpesvirus proteins. Proc Natl Acad Sci U S A 104:7241–7246. https://doi.org/10.1073/pnas.0701757104.
17. Hollinshead M, Johns HL, Sayers CL, Gonzalez-Lopez C, Smith GL, Elliott G. 2012. Endocytic tubules regulated by Rab GTPases 5 and 11 are used for envelopment of herpes simplex virus. EMBO J 31:4204–4220. https://doi.org/10.1038/emboj.2012.262.
18. Harley CA, Dasgupta A, Wilson DW. 2001. Characterization of herpes simplex virus-containing organelles by subcellular fractionation: role for organelle acidification in assembly of infectious particles. J Virol 75:1236–1251. https://doi.org/10.1128/JVI.75.3.1236-1251.2001.
19. Johns HL, Gonzalez-Lopez C, Sayers CL, Hollinshead M, Elliott G. 2014. Rab6 dependent post-Golgi trafficking of HSV1 envelope proteins to sites of virus envelopment. Traffic 15:157–178. https://doi.org/10.1111/tra.12134.
20. Albecka A, Laine RF, Janssen AF, Kaminski CF, Crump CM. 2016. HSV-1 glycoproteins are delivered to virus assembly sites through dynamin-dependent endocytosis. Traffic 17:21–39. https://doi.org/10.1111/tra.12340.
21. Szilagyi JF, Cunningham C. 1991. Identification and characterization of a novel non-infectious herpes simplex virus-related particle. J Gen Virol 72(Part 3):661–668. https://doi.org/10.1099/0022-1317-72-3-661.
22. McLauchlan J, Rixon FJ. 1992. Characterization of enveloped tegument structures (L particles) produced by alphaherpesviruses: integrity of the tegument does not depend on the presence of capsid or envelope. J Gen Virol 73:269–276. https://doi.org/10.1099/0022-1317-73-2-269.
23. Alemañ N, Quiroga MI, López-Peña M, Vázquez S, Guerrero FH, Nieto JM. 2003. L-particle production during primary replication of pseudorabies virus in the nasal mucosa of swine. J Virol 77:5657–5667. https://doi.org/10.1128/JVI.77.10.5657-5667.2003.
24. Dargan DJ, Patel AH, Subak-Sharpe JH. 1995. PREPs: herpes simplex virus type 1-specific particles produced by infected cells when viral DNA replication is blocked. J Virol 69:4924–4932.
25. Carpenter JE, Hutchinson JA, Jackson W, Grose C. 2008. Egress of light particles among filopodia on the surface of varicella-zoster virus-infected cells. J Virol 82:2821–2835. https://doi.org/10.1128/JVI.01821-07.
26. Ibiricu I, Maurer UE, Grünewald K. 2013. Characterization of herpes simplex virus type 1 L-particle assembly and egress in hippocampal neurones by electron cryo-tomography. Cell Microbiol 15:285–291. https://doi.org/10.1111/cmi.12093.
27. Owen DJ, Crump CM, Graham SC. 2015. Tegument assembly and secondary envelopment of alphaherpesviruses. Viruses 7:5084–5114. https://doi.org/10.3390/v7092861.
28. Bucks MA, O'Regan KJ, Murphy MA, Wills JW, Courtney RJ. 2007. Herpes simplex virus type 1 tegument proteins VP1/2 and UL37 are associated with intranuclear capsids. Virology 361:316–324. https://doi.org/10.1016/j.virol.2006.11.031.
29. Coller KE, Lee JI, Ueda A, Smith GA. 2007. The capsid and tegument of the alphaherpesviruses are linked by an interaction between the UL25 and VP1/2 proteins. J Virol 81:11790–11797. https://doi.org/10.1128/JVI.01113-07.
30. Maringer K, Stylianou J, Elliott G. 2012. A network of protein interactions around the herpes simplex virus tegument protein VP22. J Virol 86:12971–12982. https://doi.org/10.1128/JVI.01913-12.
31. Stylianou J, Maringer K, Cook R, Bernard E, Elliott G. 2009. Virion incorporation of the herpes simplex virus type 1 tegument protein VP22 occurs via glycoprotein E-specific recruitment to the late secretory pathway. J Virol 83:5204–5218. https://doi.org/10.1128/JVI.00069-09.
32. Fuchs W, Klupp BG, Granzow H, Hengartner C, Brack A, Mundt A, Enquist LW, Mettenleiter TC. 2002. Physical interaction between envelope glycoproteins E and M of pseudorabies virus and the major tegument protein UL49. J Virol 76:8208–8217. https://doi.org/10.1128/JVI.76.16.8208-8217.2002.
33. Han J, Chadha P, Meckes DG, Jr, Baird NL, Wills JW. 2011. Interaction and interdependent packaging of tegument protein UL11 and glycoprotein e of herpes simplex virus. J Virol 85:9437–9446. https://doi.org/10.1128/JVI.05207-11.
34. Fuchs W, Granzow H, Mettenleiter TC. 2003. A pseudorabies virus recombinant simultaneously lacking the major tegument proteins encoded by the UL46, UL47, UL48, and UL49 genes is viable in cultured cells. J Virol 77:12891–12900. https://doi.org/10.1128/JVI.77.23.12891-12900.2003.
35. Zhang Y, McKnight JL. 1993. Herpes simplex virus type 1 UL46 and UL47 deletion mutants lack VP11 and VP12 or VP13 and VP14, respectively, and exhibit altered viral thymidine kinase expression. J Virol 67:1482–1492.
36. Elliott G, Hafezi W, Whiteley A, Bernard E. 2005. Deletion of the herpes simplex virus VP22-encoding gene (UL49) alters the expression, localization, and virion incorporation of ICP0. J Virol 79:9735–9745. https://doi.org/10.1128/JVI.79.15.9735-9745.2005.
37. Lobanov VA, Maher-Sturgess SL, Snider MG, Lawman Z, Babiuk LA, van Drunen Littel-van den Hurk S. 2010. A UL47 gene deletion mutant of bovine herpesvirus type 1 exhibits impaired growth in cell culture and lack of virulence in cattle. J Virol 84:445–458. https://doi.org/10.1128/JVI.01544-09.
38. Carpenter DE, Misra V. 1991. The most abundant protein in bovine herpes 1 virions is a homologue of herpes simplex virus type 1 UL47. J Gen Virol 72(Part 12):3077–3084. https://doi.org/10.1099/0022-1317-72-12-3077.
39. Harland J, Dunn P, Cameron E, Conner J, Brown SM. 2003. The herpes simplex virus (HSV) protein ICP34.5 is a virion component that forms a DNA-binding complex with proliferating cell nuclear antigen and HSV replication proteins. J Neurovirol 9:477–488. https://doi.org/10.1080/13550280390218788.
40. Roller RJ, Roizman B. 1992. The herpes simplex virus 1 RNA binding protein US11 is a virion component and associates with ribosomal 60S subunits. J Virol 66:3624–3632.
41. Engel EA, Song R, Koyuncu OO, Enquist LW. 2015. Investigating the biology of alpha herpesviruses with MS-based proteomics. Proteomics 15:1943–1956. https://doi.org/10.1002/pmic.201400604.
42. Choi DS, Kim DK, Kim YK, Gho YS. 2015. Proteomics of extracellular

vesicles: exosomes and ectosomes. Mass Spectrom Rev 34:474–490. https://doi.org/10.1002/mas.21420.
43. Wang M, Herrmann CJ, Simonovic M, Szklarczyk D, von Mering C. 2015. Version 4.0 of PaxDb: protein abundance data, integrated across model organisms, tissues, and cell-lines. Proteomics 15:3163–3168. https://doi.org/10.1002/pmic.201400441.
44. Thompson A, Schäfer J, Kuhn K, Kienle S, Schwarz J, Schmidt G, Neumann T, Hamon C. 2003. Tandem mass tags: a novel quantification strategy for comparative analysis of complex protein mixtures by MS/MS. Anal Chem 75:1895–1904. https://doi.org/10.1021/ac0262560.
45. Thurlow JK, Rixon FJ, Murphy M, Targett-Adams P, Hughes M, Preston VG. 2005. The herpes simplex virus type 1 DNA packaging protein UL17 is a virion protein that is present in both the capsid and the tegument compartments. J Virol 79:150–158. https://doi.org/10.1128/JVI.79.1.150-158.2005.
46. Maresova L, Pasieka TJ, Homan E, Gerday E, Grose C. 2005. Incorporation of three endocytosed varicella-zoster virus glycoproteins, gE, gH, and gB, into the virion envelope. J Virol 79:997–1007. https://doi.org/10.1128/JVI.79.2.997-1007.2005.
47. Krzyzaniak M, Mach M, Britt WJ. 2007. The cytoplasmic tail of glycoprotein M (gpUL100) expresses trafficking signals required for human cytomegalovirus assembly and replication. J Virol 81:10316–10328. https://doi.org/10.1128/JVI.00375-07.
48. Kropff B, Koedel Y, Britt W, Mach M. 2010. Optimal replication of human cytomegalovirus correlates with endocytosis of glycoprotein gpUL132. J Virol 84:7039–7052. https://doi.org/10.1128/JVI.01644-09.
49. Ferguson SM, Raimondi A, Paradise S, Shen H, Mesaki K, Ferguson A, Destaing O, Ko G, Takasaki J, Cremona O, O'Toole E, De Camilli P. 2009. Coordinated actions of actin and BAR proteins upstream of dynamin at endocytic clathrin-coated pits. Dev Cell 17:811–822. https://doi.org/10.1016/j.devcel.2009.11.005.
50. Foster TP, Chouljenko VN, Kousoulas KG. 2008. Functional and physical interactions of the herpes simplex virus type 1 UL20 membrane protein with glycoprotein K. J Virol 82:6310–6323. https://doi.org/10.1128/JVI.00147-08.
51. Foster TP, Melancon JM, Olivier TL, Kousoulas KG. 2004. Herpes simplex virus type 1 glycoprotein K and the UL20 protein are interdependent for intracellular trafficking and trans-Golgi network localization. J Virol 78:13262–13277. https://doi.org/10.1128/JVI.78.23.13262-13277.2004.
52. Le Sage V, Jung M, Alter JD, Wills EG, Johnston SM, Kawaguchi Y, Baines JD, Banfield BW. 2013. The herpes simplex virus 2 UL21 protein is essential for virus propagation. J Virol 87:5904–5915. https://doi.org/10.1128/JVI.03489-12.
53. Sarfo A, Starkey J, Mellinger E, Zhang D, Chadha P, Carmichael J, Wills JW. 2017. The UL21 tegument protein of herpes simplex virus 1 is differentially required for the syncytial phenotype. J Virol 91:e01167-17. https://doi.org/10.1128/JVI.01161-17.
54. Gao J, Hay TJM, Banfield BW. 2017. The product of the herpes simplex virus 2 UL16 gene is critical for the egress of capsids from the nuclei of infected cells. J Virol 91:e00350-17. https://doi.org/10.1128/JVI.00350-17.
55. Starkey JL, Han J, Chadha P, Marsh JA, Wills JW. 2014. Elucidation of the block to herpes simplex virus egress in the absence of tegument protein UL16 reveals a novel interaction with VP22. J Virol 88:110–119. https://doi.org/10.1128/JVI.02555-13.
56. Gao J, Yan X, Banfield BW. 2018. Comparative analysis of UL16 mutants derived from multiple strains of herpes simplex virus 2 (HSV-2) and HSV-1 reveals species-specific requirements for the UL16 protein. J Virol 92:e00629-18. https://doi.org/10.1128/JVI.00629-18.
57. Robinson KE, Meers J, Gravel JL, McCarthy FM, Mahony TJ. 2008. The essential and non-essential genes of bovine herpesvirus 1. J Gen Virol 89:2851–2863. https://doi.org/10.1099/vir.0.2008/002501-0.
58. Lam N, Letchworth GJ. 2000. Bovine herpesvirus 1 U(L)3.5 interacts with bovine herpesvirus 1 alpha-transinducing factor. J Virol 74:2876–2884. https://doi.org/10.1128/JVI.74.6.2876-2884.2000.
59. Rixon FJ, Addison C, McLauchlan J. 1992. Assembly of enveloped tegument structures (L particles) can occur independently of virion maturation in herpes simplex virus type 1-infected cells. J Gen Virol 73:277–284. https://doi.org/10.1099/0022-1317-73-2-277.
60. Klupp BG, Granzow H, Mettenleiter TC. 2000. Primary envelopment of pseudorabies virus at the nuclear membrane requires the UL34 gene product. J Virol 74:10063–10073. https://doi.org/10.1128/JVI.74.21.10063-10073.2000.
61. Hogue IB, Scherer J, Enquist LW. 2016. Exocytosis of alphaherpesvirus virions, light particles, and glycoproteins uses constitutive secretory mechanisms. mBio 7:e00820-16. https://doi.org/10.1128/mBio.00820-16.
62. Yang TY, Courtney RJ. 1995. Influence of the host cell on the association of ICP4 and ICP0 with herpes simplex virus type 1. Virology 211:209–217. https://doi.org/10.1006/viro.1995.1393.
63. Barreca C, O'Hare P. 2004. Suppression of herpes simplex virus 1 in MDBK cells via the interferon pathway. J Virol 78:8641–8653. https://doi.org/10.1128/JVI.78.16.8641-8653.2004.
64. Barreca C, O'Hare P. 2006. Characterization of a potent refractory state and persistence of herpes simplex virus 1 in cell culture. J Virol 80:9171–9180. https://doi.org/10.1128/JVI.00962-06.
65. McLauchlan J, Addison C, Craigie MC, Rixon FJ. 1992. Noninfectious L-particles supply functions which can facilitate infection by HSV-1. Virology 190:682–688. https://doi.org/10.1016/0042-6822(92)90906-6.
66. Su C, Zhan G, Zheng C. 2016. Evasion of host antiviral innate immunity by HSV-1, an update. Virol J 13:38. https://doi.org/10.1186/s12985-016-0495-5.
67. Deschamps T, Kalamvoki M. 2017. Evasion of the STING DNA-sensing pathway by VP11/12 of herpes simplex virus 1. J Virol 91:e00535-17. https://doi.org/10.1128/JVI.00535-17.
68. Afroz S, Brownlie R, Fodje M, van Drunen Littel-van den Hurk S. 2016. VP8, the major tegument protein of bovine herpesvirus 1, interacts with cellular STAT1 and inhibits interferon beta signaling. J Virol 90:4889–4904. https://doi.org/10.1128/JVI.00017-16.
69. Elliott G, O'Hare P. 1999. Live-cell analysis of a green fluorescent protein-tagged herpes simplex virus infection. J Virol 73:4110–4119.
70. Elliott G, O'Hare P. 1997. Intercellular trafficking and protein delivery by a herpesvirus structural protein. Cell 88:223–233. https://doi.org/10.1016/S0092-8674(00)81843-7.
71. Verhagen J, Hutchinson I, Elliott G. 2006. Nucleocytoplasmic shuttling of bovine herpesvirus 1 UL47 protein in infected cells. J Virol 80:1059–1063. https://doi.org/10.1128/JVI.80.2.1059-1063.2006.
72. Sayers CL, Elliott G. 2016. Herpes simplex virus 1 enters human keratinocytes by a nectin-1-dependent, rapid plasma membrane fusion pathway that functions at low temperature. J Virol 90:10379–10389. https://doi.org/10.1128/JVI.01582-16.